The Astrophysical Journal, 635:1329–1347, 2005 December 20

CHANDRA OBSERVATIONS OF COMET 2P/ENCKE 2003: FIRST DETECTION OF A COLLISIONALLY THIN, FAST SOLAR WIND CHARGE EXCHANGE SYSTEM

C. M. Lisse,[1,2] D. J. Christian,[3] K. Dennerl,[4] S. J. Wolk,[5] D. Bodewits,[6] R. Hoekstra,[6]
M. R. Combi,[7] T. Mäkinen,[8] M. Dryer,[9] C. D. Fry,[10] and H. Weaver[1]

Received 2005 May 20; accepted 2005 August 24

ABSTRACT

We report the results of 15 hr of *Chandra* observations of comet 2P/Encke 2003 on November 24. X-ray emission from comet Encke was resolved on scales of 500–40,000 km, with unusual morphology due to the presence of a low-density, collisionally thin (to charge exchange) coma. A light curve with peak-to-peak amplitude of 20% consistent with a nucleus rotational period of 11.1 hr was found, further evidence for a collisionally thin coma. We confirm emission lines due to oxygen and neon in the 800–1000 eV range but find very unusual oxygen and carbon line ratios in the 200–700 eV range, evidence for low-density, high effective temperature solar wind composition. We compare the X-ray spectral observation results to contemporaneous measurements of the coma and solar wind made by other means and find good evidence for the dominance of a postshock bubble of expanding solar wind plasma, moving at 600 km s^{-1} with charge state composition between that of the "fast" and "slow" solar winds.

Subject headings: comets: individual (2P/Encke 2003) — solar wind — X-rays: general

Online material: color figure

1. INTRODUCTION

Cometary X-ray emission, first discovered in 1996 and now observed in over 20 comets, has been shown to be caused by charge exchange reactions between highly charged solar wind minor ions (~0.1% of all solar wind ions) and neutral gas species emitted by the nucleus into the cometary coma (Cravens 1997; Dennerl et al. 1997; Kharchenko & Dalgarno 2000, 2001; Krasnopolsky et al. 2002; Lisse et al. 1999, 2001). The emission appears to be confined to the sunward hemisphere of the neutral coma, with emission-line energies characteristic of atomic cascades from hydrogen-like and helium-like C, N, O, and Ne and a luminosity proportional to the solar wind ion flux density.

The implications of the charge exchange mechanism are manyfold and have yet to be fully explored. Variations in the emission that track spatial, temporal, and compositional changes in the solar wind should be present. The solar wind has large-scale structure relating to the very different corona environments at the equator and pole of the Sun: the low-latitude solar wind is relatively dense, slow moving ($v \sim 200$–300 km s^{-1}), and of high temperature ($\sim 2 \times 10^6$ K), while the high-latitude polar wind is less dense and cooler ($\sim 1 \times 10^6$ K) but moving at higher average speeds ($v > 400$ km s^{-1}). These differences should cause detectable differences in the observed X-ray spectrum of the comet (Beiersdorfer et al. 2003; Bodewits et al. 2004). Limitations of the emission region to the volume of the neutral coma available to the solar wind are predicted, with evidence in the morphology and size of the emission region (Lisse & Christian 2002; Lisse et al. 2004; Wegmann et al. 2004). Modulation of the X-ray signal due to modulations of the neutral coma density should be present for systems that are collisionally thin. The coma neutral density is modulated as actively subliming emitting regions on the cometary nucleus rotate in and out of sunlight during the course of a comet's day.

To date, the best-observed comets in the X-ray have been close Earth approachers with high coma "activity" (i.e., rate of sublimation of volatile ices into neutral gas species in the gravitationally unbound atmosphere surrounding the nucleus). The brightest known comet target available during *Chandra* Cycle 5 was 2P/Encke 2003 (hereafter Encke), an old, short-period comet with a low production rate of dust and gas. Well observed for ~60 apparitions over the course of three centuries, the comet had a very close passage by the Earth in 2003 November–December, with a minimum Earth-comet distance of 0.26 AU and a maximum visual brightness of $V \sim 6.4$. In 1997, at larger heliocentric and similar geocentric distance and a magnitude fainter brightness, we found Encke to be an excellent laboratory for studies of cometary X-ray emission (Lisse et al. 1999). With only broadband photometry, we were able to infer that charge exchange between highly ionized solar wind minor ions and cometary neutral gas species was the most likely emission mechanism (Lisse et al. 1999).

The highly favorable perigee passage of comet Encke in late 2003 provided an excellent opportunity to use *Chandra*'s spatial, spectral, and temporal resolution to study cometary X-ray emission in the low neutral target density, low X-ray flux regime. The 1997 findings suggested a straightforward *Chandra* experiment: continuous ACIS-S observations of Encke throughout one

[1] Planetary Exploration Group, Space Department, Johns Hopkins University Applied Physics Laboratory, 11100 Johns Hopkins Road, Laurel, MD 20723; carey.lisse@jhuapl.edu, hal.weaver@jhuapl.edu.
[2] Corresponding author.
[3] Queens University, Department of Pure and Applied Physics, Belfast BT7 1NN, UK; d.christian@qub.ac.uk.
[4] Max-Planck-Institut für extraterrestrische Physik, Postfach 1603, 85740 Garching, Germany; kod@mpe.mpg.de.
[5] *Chandra X-Ray Observatory* Center, Harvard-Smithsonian Center for Astrophysics, 60 Garden Street, Cambridge, MA 02138; swolk@cfa.harvard.edu.
[6] KVI Atomic Physics, Rijkuniversiteit Groningen, Zernikelaan 25, 9747 AA Groningen, Netherlands; bodewits@kvi.nl, hoekstra@kvi.nl.
[7] Department of Atmospheric, Oceanic, and Space Sciences, University of Michigan, 2455 Hayward Street, Ann Arbor, MI 48109-2143; mcombi@engin.umich.edu.
[8] Finnish Meteorological Institute, Space Research, P.O. Box 503, FIN-00101 Helsinki, Finland; teemu.makinen@fmi.fi.
[9] NOAA Space Environment Center, 325 Broadway, Boulder, CO 80305; murray.dryer@noaa.gov.
[10] Exploration Physics International, Inc., Suite 37-105, 6275 University Drive, Huntsville, AL 35806-1776; gfry@expi.com.

nuclear revolution period of 15 hr (as determined by Luu & Jewitt 1990) during the time of its closest approach to Earth. Encke is the first low-activity, low-dust, short-period comet observed by *Chandra*, and the first comet observed in the X-ray on more than one perihelion passage, allowing us to check for reproducibility in cometary X-ray emission behavior and providing an important bridge between the *Chandra* and *ROSAT*/*EUVE* (*Röntgensatellit*/*Extreme Ultraviolet Explorer*) comet databases.

In this paper, we report the results of our observations and compare the emission morphology and extracted X-ray spectra in the 200–1000 eV range to current models. In § 2 we describe the details of the instruments used and our data analysis techniques. In § 3 we present the observational results, placing them in the context of previous cometary X-ray observations. In § 4 we compare the observations to contemporaneous measurements of the coma and solar wind made by other means and argue for the presence of a low-density, collisionally thin (to charge exchange) coma and a fast moderate-density solar wind as a plausible physical model explaining our results. In § 5 we list our observational and model-derived conclusions for X-ray emission from Encke in 2003.

2. INSTRUMENTAL

Chandra.—*Chandra* observations of comet Encke were obtained on 2003 November 24 in 15 hr (54 ks) of continuous pointing, using the ACIS-S CCD spectral array, which combines the abilities to image X-rays with a plate scale of $0\farcs5$ pixel^{-1} and to produce accurate, moderate-resolution spectra ($\Delta E \sim 110$ eV FWHM, $\Delta E_{\rm Gaussian} = 49$ eV) from 0.30 to 2.0 keV. During the *Chandra* observation on 2003 November 24, Encke was approximately 0.88 AU from the Sun and 0.27 AU from the Earth, with a total visual magnitude of $V \sim 6.5$, a total luminosity of $L_{\rm optical} \sim 2 \times 10^{19}$ ergs s^{-1}, and an estimated $Q_{\rm gas}$ of $\sim 2 \times 10^{28}$ mol s^{-1}.

We obtained 30 pointed *Chandra* observations of Encke on 2003 November 24 from 04:30 to 18:30 UT. The method of *Chandra* observation was kept simple: the ACIS-S array was pointed on the sky $2'$ in front of the comet along the direction of its apparent motion, and the comet was allowed to move through the field of view. No active guiding on the comet was attempted. *Chandra* observations return a list of time-tagged detections of individual photon pulse heights and spatial locations. *Chandra* was able to follow the comet's nonsidereal motion using multiple pointings, and the target was centered in the back-illuminated CCD chip S3, the most sensitive CCD for energies below 1 keV. No obvious bright background sources were detected in our data, other than the comet.

Using the `sso_freeze` algorithm, part of the *Chandra* Interactive Analysis of Observations (CIAO) software, we constructed a comet image remapped onto a coordinate system moving with the comet. The resulting effective field of view of the observations in the cometocentric coordinate system is $10' \times 10'$. Background removal was performed in two different ways: (1) counting all photons within a circular aperture of $550''$ and subtracting the signal measured in an annular radius of $200''$ outside this using the CIAO reduction package, and (2) creating a signal versus aperture width curve using IDL, after removing a background estimated from a "frame" 20 pixels wide around the edge of the field of view in cometocentric coordinates. The two methods agree to within 20% in the amount of background counts per pixel. A total of 6500 photons attributable to the comet were found after spatial background removal using XSPEC fitting routines (Arnaud 1996), for an average count rate over the 54 ks of observations of 0.12 counts s^{-1}. To create light curves, a circular source aperture of $3\farcm7$ radius was chosen in CIAO, and several background apertures were extracted $>4'$ away from the comet's diffuse emission and toward the outer edge of the chip. Spectra were extracted in an identical fashion, and the effect of energy-dependent instrument sensitivity was removed using the latest effective areas given in the *Chandra* on-orbit measured instrument response matrices. Upon examination of the extracted spectra, only photons of energy 0.20–1.0 keV were found to be statistically significant against the sky and instrumental backgrounds.

SOHO and ACE.—*SOHO* (*Solar and Heliospheric Observatory*) measurements of the solar wind proton flux, solar soft X-ray flux, and solar wind magnetic field were obtained using the CELIAS instrument.[11] *ACE* (*Advanced Composition Explorer*) ULEIS ultrasoft ion spectroscopy data for H, He^4, C, O, Ne, and Fe were also used.[12] Our observations of Encke using the ACIS-S camera and of the solar-terrestrial environment using *SOHO*, *Wind*, and *ACE* were performed in the same manner as used to observe comets C/1999 S4 (LINEAR) (Lisse et al. 2001) and C/McNaught-Hartley 1999 T1 (Krasnopolsky et al. 2002). We refer the reader to these papers for detailed descriptions of the instruments used and the corrections applied to the data.

3. OBSERVATIONS

Morphology.—The emission morphology (Fig. 1*a*) is decidedly non–crescent shaped, unlike the overwhelming majority of the 20+ comets observed in the X-ray to date (Lisse et al. 2004). At the 104° phase angle of our observations, the hemispherical emission geometry consistent with an extended cometary atmosphere encountering the solar wind and fully depleting the population of minor ions in charge exchange interactions would appear as a crescent-shaped region in projection (Wegmann et al. 2004). The morphology of the emission region most closely matches the morphology of the optical coma (Figs. 1*b* and 1*c*), which is relatively faint and dominated by a sunward "fan" composed of two bright jets. For this to be the case, the limiting constituent in the two-body charge exchange interaction has to be the neutral gas coma population, not the solar wind minor ion flux. In other comets, the neutral gas coma has been collisionally thick, leading to the classical "crescent shaped" emission region between the nucleus and the Sun.

Further evidence for a relatively low rate of charge exchange interaction can be found in the overall scale of the observed emission region. The *Chandra* signal emission can be traced out to only 40,000 km ($3'$ at 0.28 AU) in radius, roughly centered around the Sun-nucleus line. Similar to the 1997 measurements, the emission region is over an order of magnitude more compact than found in other comets; 80% of the emission was found within a spherical region of radius 40,000 km from the nucleus. Previous comets have demonstrated emission out to 10^6 km, the approximate limit of the neutral gas coma.

The sunward morphology in 2003 is different from that exhibited in 1997 July (Fig. 1*d*), with the 1997 structure appearing to be somewhat more crescent shaped. However, the 1997 optical coma also appears to be denser and more uniformly distributed. Differences in the effective spatial resolution cannot be the cause, as all three observations demonstrated "seeing" on the order of $10''$, limited by instrumental capabilities and photon counting statistics (Table 1).

[11] Data obtained from http://www.usc.edu/dept/space_science/semdata97.htm and http://umtof.umd.edu/pm/crn.

[12] See http://sd-www.jhuapl.edu/ACE/ULEIS/spec_gadget.html.

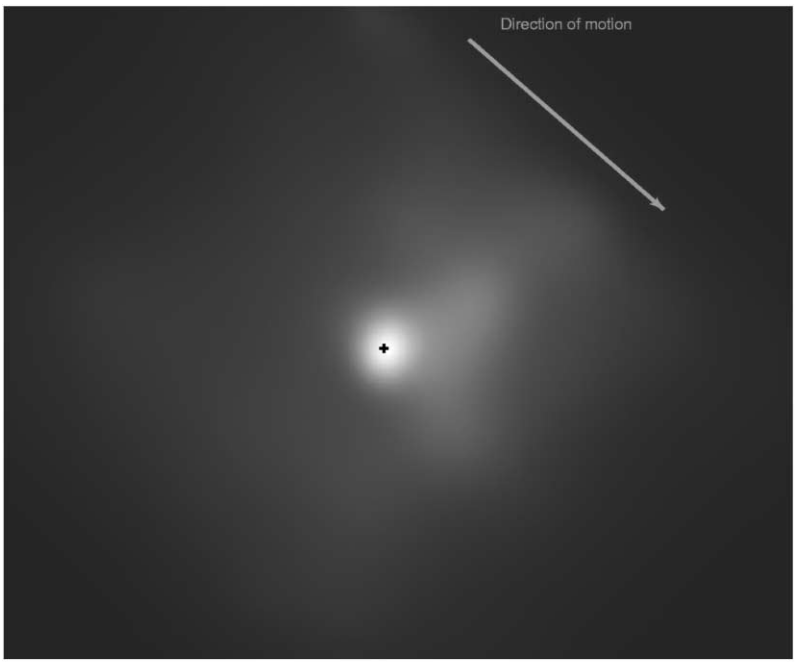

FIG. 1*a*

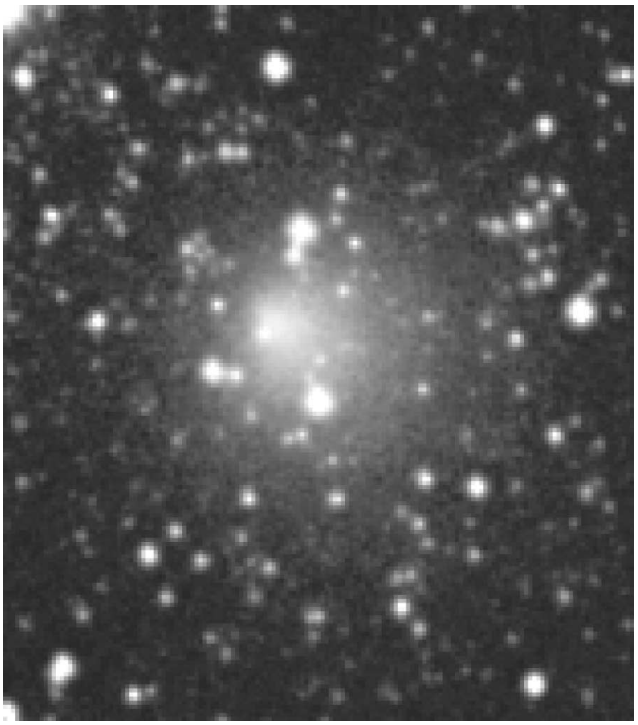

FIG. 1*b*

FIG. 1.—Morphology of the cometary X-ray emission. (*a*) Combined *Chandra* X-ray map of Encke on 2003 November 24. The photons have been reregistered from the *Chandra* detector coordinate system to a cometocentric coordinate system. North is up and east is to the left. The direction to the Sun is approximately toward the right. The arrow denotes the comet's direction of apparent motion. The cross denotes the position of the nucleus. The reconstructed field of view is $10' \times 10'$ [$(9 \times 10^4$ km$) \times (9 \times 10^4$ km)], and the pixel resolution is $10''$. (*b*) Wide-field optical green filter CCD image of the dust coma obtained by M. Jager and G. Rhemann on 2003 November 17 UT. (*c*) CN image of the gas coma on 2003 November 24 from D. Schleicher and L. Woodney. In both images, the comet exhibits a diffuse fan in the sunward direction and a centralized core of optical emission. Unlike other comets observed to date and Encke as observed in 1997 (Lisse et al. 1999), the X-ray and optical images correlate well. There is no obvious anti-sunward optical emission, nor is a tail evident. Encke appears to have been very inactive at the time of *Chandra* observation. (*d*) X-ray, *EUVE*, and optical images of Encke in 1997, after Lisse et al. (1999). *Left*: *ROSAT* HRI 1997 July 4–8 image. *Middle*: *EUVE* Lexan B 1997 July 6–8 image. The images are in a reference frame moving with the comet's apparent sky position. The projected direction toward the Sun is to the right in each image. *Right*: Visible-light image of the comet taken on 1997 June 4 UT, demonstrating a coma with asymmetric emission and a weak tail. The coordinate system and length scale of 1300 km/$10''$ pixel are the same in all three images. (*e*) Spatial profiles in the north-south direction, perpendicular to the nucleus-Sun line, for the X-ray emission (*diamonds*) and for the CN/OH gas coma fluorescence (*solid line*) and dust coma continuum scattered radiation (*dashed line*) from CCD imagery obtained at the Lowell 42 inch (1 m) telescope by D. Schleicher and L. Woodney in 2003. The X-ray emission profile, while noisy, tracks the $\sim 1/\rho$ gas emission out to large distances, while the dust emission decreases much more rapidly in the core region. Here $3' = 40{,}000$ km, and the maximum offset between the peaks of the gas coma flux and the X-ray flux is within $2''$, or 450 km. [*See the electronic edition of the Journal for a color version of* (*a*).]

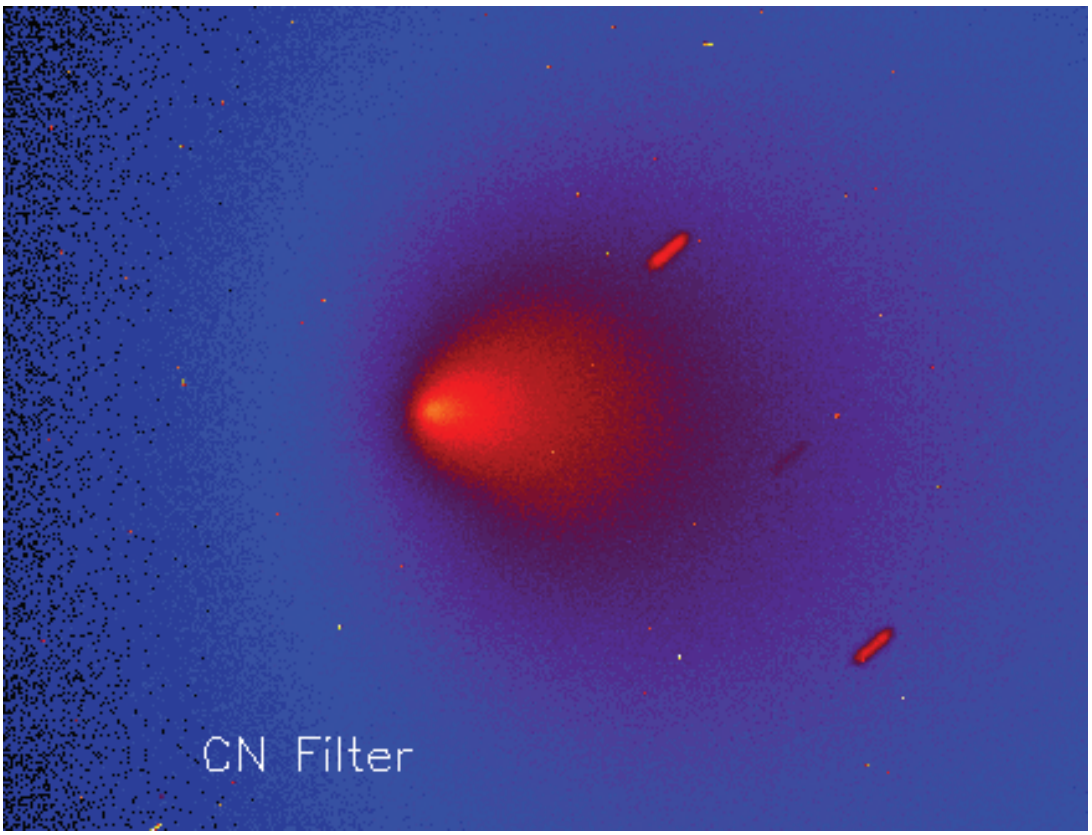

FIG. 1*c*

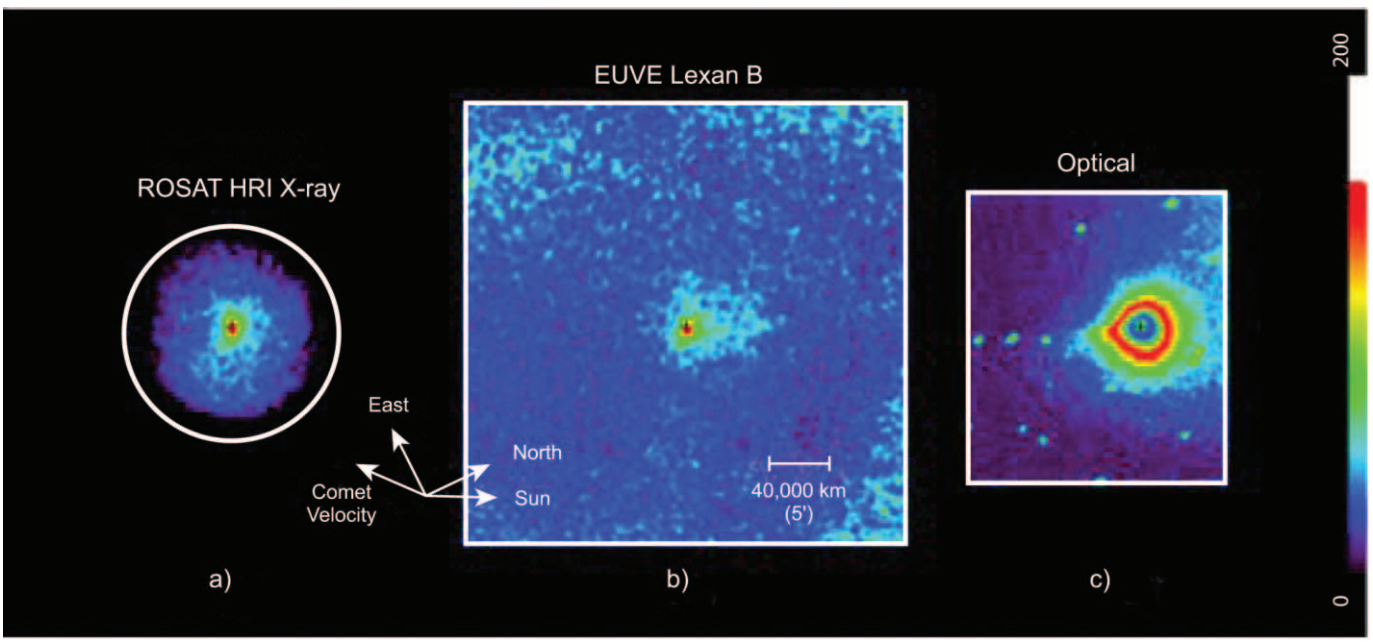

FIG. 1*d*

With the comet at 0.27 AU from the Earth, 1″ corresponded to 215 km at the nucleus, so the theoretical *Chandra* resolution at the comet was 100 km pixel^{-1}. However, the actual size of a statistically significant spatial resolution element was determined by the limited number of photons detected. In regions of high net signal, e.g., near the nucleus, this resolution was on the order of 2″ (430 km) per resolution element. The average photon-limited effective pixel size realized over the detected X-ray emission region was 7″ (1500 km) per resolution element.

Light curve.—The source had a total of 6500 counts in the 300–1000 eV energy range after background removal, corresponding to a total 0.3–1.0 keV X-ray luminosity L_X of 3.8×10^{14} ergs s^{-1} and $E_{photon} = 450$ eV (and an average *Chandra* effective area of 50 cm^2). This is similar to the 4×10^{14} ergs s^{-1}

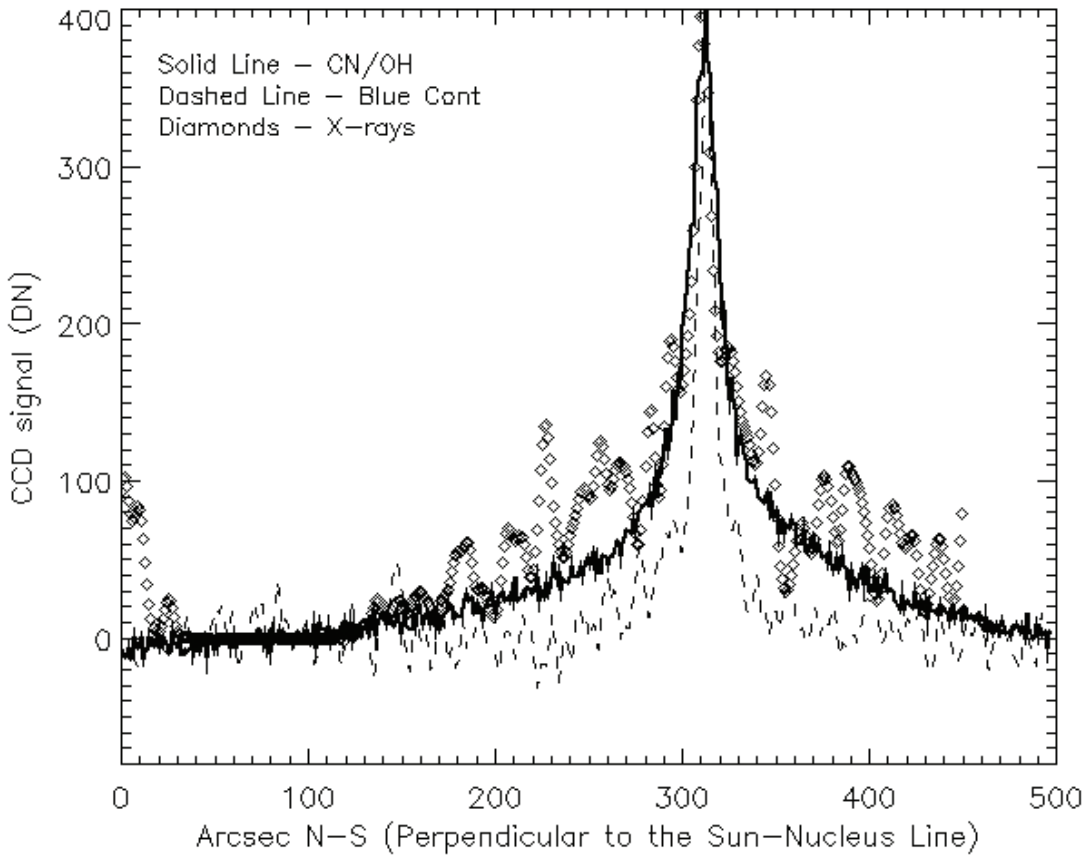

FIG. 1*e*

found for Encke in 1997 using the *ROSAT* HRI from 0.10 to 0.50 keV, with an average photon energy of 0.23 keV. (N.B., the *ROSAT* observations, being insensitive to the bright cometary emission lines from 0.5 to 0.8 keV, probably underestimated the *Chandra* luminosity by about a factor of 3; see Fig. 3.) The realized *Chandra* count rate is roughly 1 order of magnitude lower than expected, due to a combination of the degraded *Chandra* soft X-ray system response in Cycle 5 from focal plane surface contamination, the low solar wind flux density at the time of observation, and the relatively low level of cometary outgassing activity at the time of observation. The average total count rate, after background removal, was $\sim$0.12 counts s^{-1}.

A light curve for the *Chandra* observations on 2003 November 24 was created by binning all the 300–1000 eV events in a 40,000 km radius aperture into 30 discrete intervals, corresponding to the 30 pointings of the spacecraft performed during the 15 hr of on-target time (Fig. 2*a*). The linearly decreasing trend seen in the solar wind flux (solar wind flux = density $\times$ velocity; Fig. 4*c*) was then removed. The resulting light curve demonstrates a periodicity at 10.5 $\pm$ 1.5 hr (2 σ) and a peak-to-peak amplitude of 20%. The majority of the error found in our light curve measurements was due to fluctuations of the background and in fitting the solar wind flux trend with time. We are able to rule out the null variation case (periodicity = 0 hr) at the 95% confidence limit. The variation of the background signal removed from the observations does not show any periodicity. None of the impulsive events found in our previous observations of comets was seen (Lisse et al. 1996, 1999, 2001).

Spectroscopy.—The *Chandra* ACIS-S spectra (extracted from a circular aperture 3.′7 or 43,000 km in radius, centered on the nucleus position) show clear evidence of line emission at the appropriate energies for hydrogen-like and helium-like C, N, O,

TABLE 1
OBSERVATION TIMES AND OBSERVING PARAMETERS

Comet	Observation Time (UT)	r_h (AU)	Δ (AU)	Phase (deg)	Heliographic Latitude (deg)	Heliographic Longitude (deg)	Q_{gas} (mol s^{-1})	Telescope and Instrument	Energy (keV)	Measured Extent (km)
2P/Encke 1997.....	1997 Jul 4–9	0.98–1.07	0.191–0.203	93.3–69.6	−4	−3.9	1.5×10^{28}	*ROSAT* HRI, *EUVE* MCP	0.025–0.80	$\sim 5 \times 10^4$
2P/Encke 2003.....	2003 Nov 24	0.888	0.276	103	14.4	−9.6	7.3×10^{27}	*Chandra* ACIS-S CCD	0.20–2.0	$\sim 4 \times 10^4$

NOTES.—Position, gas production rate, and approximate radial extent of the observed X-ray emission for Encke in 1997 and 2003. Here r_h is the comet-Sun distance, Δ is the comet-Earth distance, the heliographic latitude and Δlongitude = (longitude$_{comet}$ − longitude$_{Earth}$) are the comet's position as seen from the Sun, and Q_{gas} is the gas production rate from the nucleus surface (Wegmann et al. 2004; T. Mäkinen 2004, private communication).

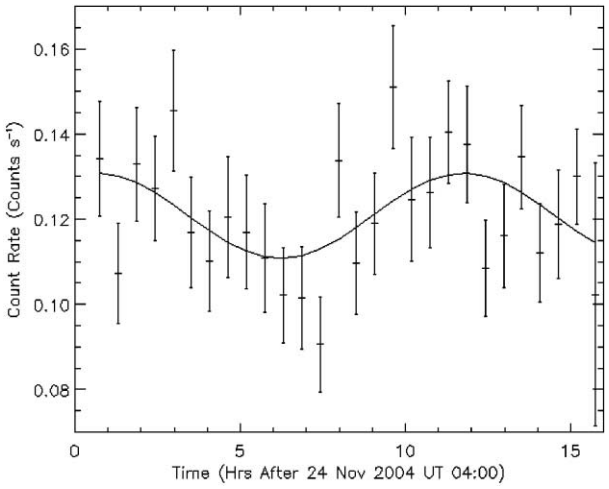

FIG. 2*a*

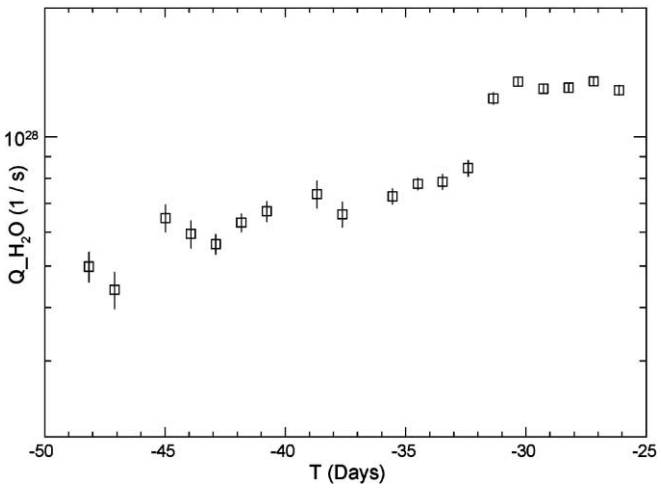

FIG. 2*b*

FIG. 2.—Time dependence of the X-ray emission. (*a*) Total 0.3–1.0 keV count rate vs. time, grouped by the 30 pointings of the spacecraft on the comet. *Dashes*: Observed count rate, with solar wind flux trend removed. Plotted error bars are 1 σ. *Solid curve*: Best-fit light curve using the 11.1 hr period of Fernández et al. (2005) and Belton et al. (2005). The best-fit X-ray sinusoid has a 20% (peak to peak) amplitude, compared to the mean of 0.121 counts s^{-1}, and a χ^2_ν of 1.04, compared to 1.4 for no variation with time, which can be rejected at the 98% CL. (*b*) Time dependence of the water gas production from the comet, as determined from *SOHO* SWAN observations of the Lyα emission. The day of the *Chandra* observations, 2003 November 24, corresponds to 36 days before perihelion on this plot. During this time, the water production was monotonically increasing as the comet approached the Sun.

and Ne solar wind ions (Fig. 3, Table 2). The strongest and most easily resolved emission in the Encke spectrum, as in other cometary spectra (Lisse et al. 2001; Krasnopolsky et al. 2002), are due to the O VII charge exchange complex at 550–580 eV, the O VII/O VIII charge exchange lines at ~660 eV, the O VIII lines at 780 and 830 eV, the C VI and C V charge exchange lines at 368 and 308 eV, the NV VIII/C VI line complex at 430–480 eV, and the 940 eV Ne IX charge exchange line. Comparison of the measured line centers in Table 2 and the theoretical line energies shows agreement between the predicted and measured line energies within the measurement accuracy, ~0.05 keV, of the ACIS-S. The *Chandra* spectrum is consistent with the broadband X-ray photometry obtained in 1997 for comet Encke using *ROSAT* and *EUVE* (Lisse et al. 1999).

While the best model fit to the data was found for a model with eight emission lines due to C, N, O, and Ne, similar models with slightly different mixes of emission lines + continuum were also allowable fits to the data, at the 95% CL (Table 2). Despite the *Chandra* results on comets C/1999 S4 (LINEAR) (Lisse et al. 2001) and C/McNaught-Hartley 2001 (Krasnopolsky et al. 2002; Kharchenko et al. 2003), it is still not clear how many charge exchange lines are readily detectable in the 250–1000 eV energy range. While the C/1999 S4 (LINEAR) and C/McNaught-Hartley 2001 results clearly show line emission due to charge exchange, they were limited by photon statistics and unable to distinguish, at the 95% CL, between four- and six-line + continuum models and a MEKAL model with variable CNO abundance. Similarly, the 6500 total counts found for Encke do not allow any more elucidation of the nature of the background. At eight lines, we suspect that we have detected the maximum number of lines statistically possible in our 200–1000 eV moderate-resolution spectrum. The observed "continuum" should be understood to be the blending of many weaker lines, with possibly some small amount of true continuum emission due to thermal bremsstrahlung continuum or solar X-ray scattering.

The most striking result of the spectroscopic measurements is the strength of the C IV and C V lines in the 300–500 eV region. They are as strong as the line blend of O VII triplet + O VIII found at ~560 eV. For comets C/1999 S4 (LINEAR) and C/McNaught-Hartley 2001, the oxygen lines were ~3 times stronger than the carbon lines. From the spectrum alone, it is clear that Encke represents a very different spectral regime for cometary X-ray emission.

Other observations of 2P/Encke 2003.—An extensive series of observations of Encke were taken by the cometary community to take advantage of the exceptional 2003 apparition; these observations allow us to compare the observed X-ray emission with other properties of the comet.

SOHO SWAN.—The *SOHO* SWAN Lyα imager is a powerful tool to study the water gas production rate of comets (Mäkinen et al. 2001). Unfortunately, despite requests to the *SOHO* project, there were no pointed observations of Encke taken within several weeks of the *Chandra* observations. Instead, we were left with only SWAN full-sky images to analyze. This was not, however, a significant shortcoming since the comet was fairly bright at the time versus the background. For the first half of November up to and including November 22, the comet remained in an area of sky with very heavy UV star contamination, but fortunately it moved to a lower background region just in time for the *Chandra* event. Interestingly, on November 28 there appears to be a moderate outburst that dies off by the end of the analyzed period. Taking these issues into account, we find a water production rate of $5.2 \times 10^{27} r_h^{-2.75}$ s^{-1} for the whole *SOHO* observation period in late November of 2003, with $(7.3 \pm 0.3) \times 10^{27}$ s^{-1} for the day of the *Chandra* observation (Fig. 2*b*). While the comet's activity was low compared to a "bright" comet, it was still significantly higher than the lowest ever measured for a cometary body, circa 10^{25} s^{-1}. The water production for the comet was increasing daily through the day of the X-ray measurements, as the comet approached the Sun. No major outbursts in gas production were seen until 4 days after the *Chandra* measurements.

Spitzer Space Telescope.—W. T. Reach et al. (2004, private communication) obtained mid-infrared images of Encke before and after perihelion in 2003. While both images show a nucleus and extended dust trail, both permanent features of the comet, only the post-perihelion image shows evidence of a dust coma.

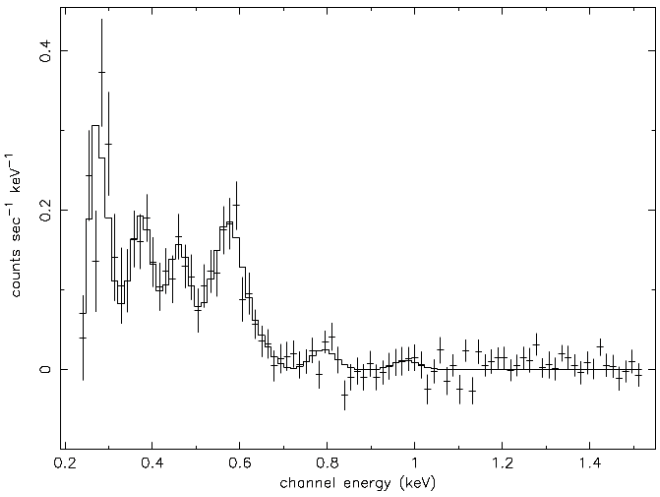

FIG. 3*a*

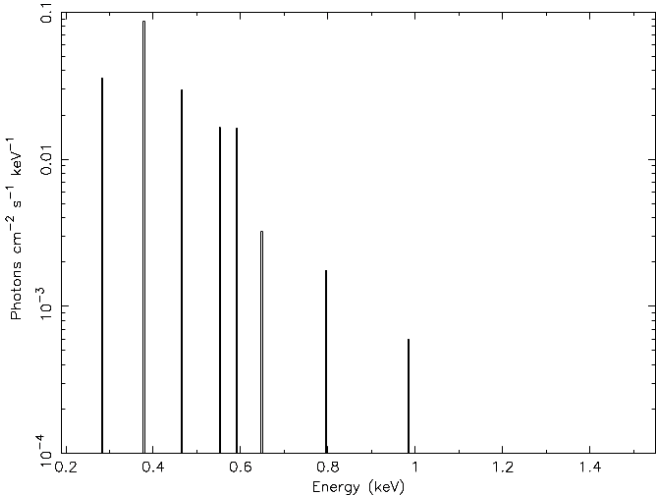

FIG. 3*b*

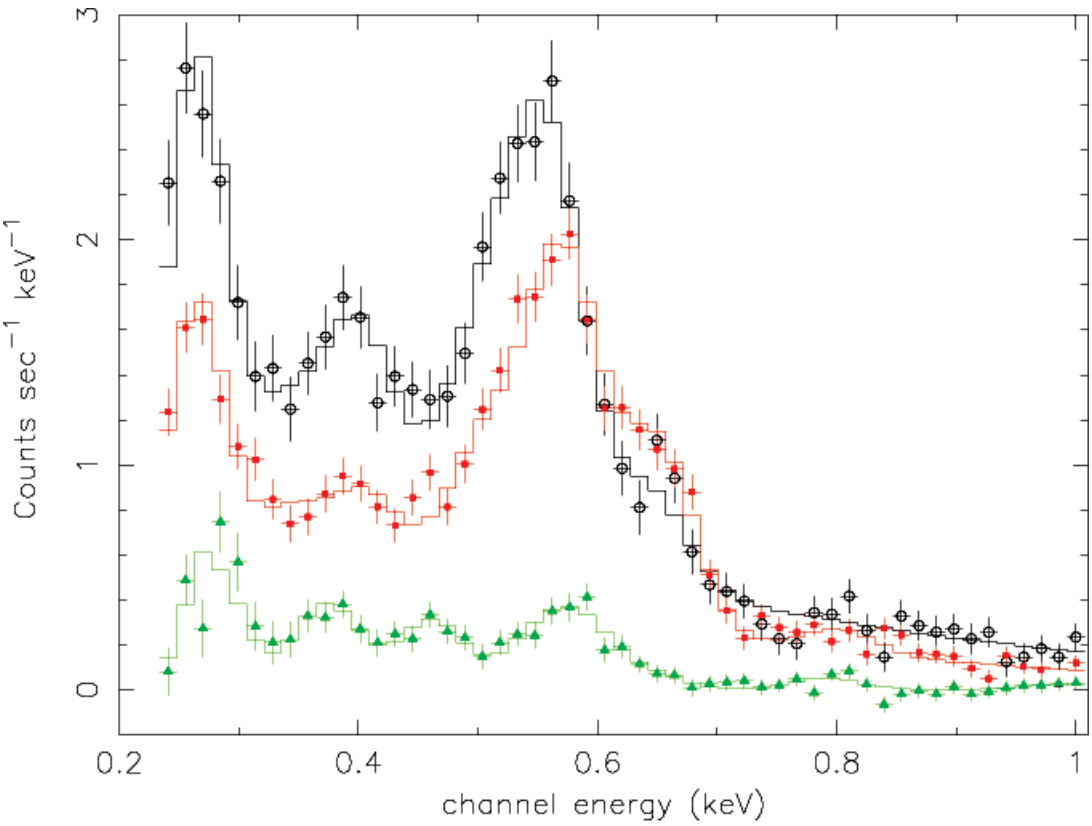

FIG. 3*c*

FIG. 3.—Spectra of the X-ray emission. (*a*) The 0.2–1.5 keV pulse-height spectrum of the 2003 November 24 X-ray emission, as measured by the ACIS-S CCD S3 chip in direct-detection mode. *Solid line*: Best eight-line model fit to the emission (see Table 2 for parameter values). As for previous comets, pronounced emission due to O VIII and O VII is evident at 560 and 660 eV. Unlike other comets, the C VI, C V, and N VI emission lines in the 200–500 eV range are as strong as the 500–700 eV O VII/O VIII lines. (*b*) Best-fit XSPEC eight-line emission model to the *Chandra* spectrum. The model lines at 284, 380, 466, 552, 590, 648, 796, and 985 are close to those predicted for charge exchange between solar wind C^{+5}, C^{+6}/N^{+6}, O^{+7}, O^{+8}, O^{+8}, and Ne^{+9} ions and neutral gases in the comet's coma. (*c*) ACIS cometary spectra of three comets. All curves show ACIS-S3 measurements with ± 1 σ error bars and the best-fit eight emission line + thermal bremsstrahlung model convolved with the ACIS-S instrument response as a histogram. *Red circles*: ACIS spectra of C/1999 S4 (LINEAR), from Lisse et al. (2001). *Black squares*: Comet McNaught-Hartley spectra, after Krasnopolsky et al. (2002). *Green triangles*: Comet 2P/Encke 2003 spectrum from this work, multiplied by a factor of 2. The C/1999 S4 (LINEAR) and C/McNaught-Hartley 2001 observations had an average count rate on the order 20 times as large, even though Encke was closer to *Chandra* and the Earth when the observations were being made. Note the 560 eV complex to 400 eV complex ratio of 2 : 3 in the bright comets.

TABLE 2
SPECTRAL MODEL FITS

MODEL	kT_{TB} (keV)	E_{line} (eV) 1	2	3	4	5	6	7	8	χ^2/dof	dof	COMMENTS
Power law	3.3 ± 0.1	...	...	...	...	...	...	...	...	5.3	57	Index free
TB	0.22 ± 0.13	...	...	...	...	...	...	...	...	4.1	57	
MEKAL	0.12 ± 0.04	...	...	...	...	...	...	...	...	3.4	57	Solar abundances
TB + four narrow lines	0.26 ± 0.07	284	380	469	570	...	...	...	...	1.2	49	Line centers free, line widths = instrument resolution
TB + four wide lines	0.27 ± 0.2	285	377	463	570	...	...	...	...	1.02	45	Line centers and widths free
TB + six lines	0.14 ± 0.1	286	375	463	532	581	636	...	...	1.08	45	Line centers free, line widths = instrument resolution
Six lines	...	283	379	464	553	600	795	...	...	0.99	47	No continuum
Eight lines	...	284	380	466	552	590	648	796	985	0.96	43	No continuum

NOTES.—Model spectral fits to the *Chandra* ACIS-S observations of 2P/Encke on 2003 November 24. Here kT_{TB} is the effective energy for the thermal bremsstrahlung continua in all models except for the power-law models, where it is the index of the power law. The quantity "dof" is the number of degrees of freedom of the fit, equivalent to the number of independent spectral channels in the *Chandra* observations minus the fit parameters. The effective hydrogen column density between *Chandra* and the comet, N_H, has been set to 10^{13} cm^{-2} for the fits, a value consistent with the estimated column between the Earth and the comet and essentially indistinguishable from zero for spectral fits of X-ray data.

As a proxy for the overall activity of the comet, the dust coma shows that Encke was much more active post-perihelion in 2003. Encke is known to have large "post-/pre-perihelion activity asymmetry" of approximately a factor of 2 (Sekanina 1988a, 1988b), most likely due to "seasonal effects" or insolation of actively emitting regions during only part of its orbit. Assuming the 2003 apparition to be representative, these active regions become more active after perihelion. The most likely explanation for this finding is that the broad sunward fan-jet, seen weakly in the pre-perihelion 2003 optical images, is much more active post-perihelion and "fills in" the sunward coma, while pre-perihelion the coma is mainly located in the two directed jets (see Festou & Barale 2000). Some of the difference in morphology and luminosity between the 1997 *ROSAT*/*EUVE* observations of the comet (taken 7 weeks after perihelion) and the 2003 *Chandra* observations of the comet (taken 6 weeks before perihelion) (Fig. 1) can then be understood as a difference in coma gas densities: there was much more neutral material, and more extension of the material in a uniform coma, in the postperihelion observations of 1997 July than the pre-perihelion observations of 2003 November.

Lowell Observatory.—As Encke was expected to be a bright comet in late 2003, D. Schleicher of Lowell Observatory included long-term narrowband photometry monitoring of Encke in his ongoing survey of comets. For our analysis, we received from their group images of the gas and dust comae of the comet in the OH, CN, and "blue continuum" filters on November 24 (Figs. 1*b* and 1*c*). In all images, the comet exhibits a diffuse fan in the sunward direction and a centralized core of optical emission. The CN and OH images are almost identical in structure, except for the much lower signal-to-noise ratio of the OH image, which is intrinsically less bright and which suffers from terrestrial atmospheric absorption. The dust coma is centered more on the nucleus and has less sunward extension than the gas coma and the X-ray emission (Fig. 1*e*). Comparing the 2003 and 1997 optical continuum images, the 2003 image shows a weaker coma with directed emission centered mainly in two jets approximately 90° apart, without any obvious tailward extension, while the 1997 image shows a well formed, rounded coma with a long, extended tail. Both images show a sunward emission asymmetry.

Solar wind characteristics at the time of the Chandra observations.—The solar wind environment at the time of observations was originally quite uncertain. Twenty-eight days before the time of observation, one of the largest X-class flares ever observed erupted from the corona, causing massive auroae on Earth and downtime for a number of spacecraft, including *Chandra*. There was much concern that 1 solar rotation (or 28 days) later, the active region responsible would rotate back toward the Earth during our observations. However, by the time of our observations, the Sun had entered a relatively quiescent phase; no solar flares are obvious in the solar X-ray flux during our observations, and *SOHO* LASCO images of the Sun are typical for a quiet Sun. There were, however, a series of small perturbations in the solar wind created by a number of coronal holes in the week before. The last perturbation of the solar wind occurred more than 3 days before our observations. Figures 4*a* and 4*b* show a simulation in the ecliptic plane of the interplanetary magnetic field polarity and solar wind velocity, density, and dynamic pressure at 00:00 and 12:00 UT on 2003 November 24 based on the studies of Dryer (1998) and Dryer et al. (2001, 2004) and the numerical procedure of Fry et al. (2001, 2003, 2004). Encke and the Earth are located in a region of low-density, fast-moving material left in the wake of the propagating shock.

The time delay observed between an element of the corotating solar wind arriving at the Earth (as measured by the near-Earth *ACE*, *SOHO*, and *Wind* spacecraft) and the observed X-ray emission from the comet can be predicted by assuming a latitude-independent solar wind flow, a quadrupole solar magnetic field, and propagation of the sector boundaries radially at the speed of the solar wind and axially with a period of one-half the solar rotation period of 28 days:

$$\Delta t_{\rm total} = \Delta t_{\rm Carr} + \Delta t_{\rm rad} = \frac{\rm longitude_{comet} - longitude_{Earth}}{14.^{\circ}7\ \rm day^{-1}} + \frac{r_{\rm comet} - r_{\rm Earth}}{v_{\rm SW} \times \left(86{,}400\ \rm s\ day^{-1}\right)}.$$

For our *Chandra* observations, we purposely chose a time when the comet was closest to the Sun in order to maximize the comet's X-ray luminosity, while keeping the phase angle of observation near 90° and the Earth-comet distance near its minimum value. This implied a comet closer to the Sun than the Earth and, for Encke, a comet that was in the retrograde sense from the Earth, earlier in the Carrington spiral than the Earth. The sum effect of the radial and longitudinal placement of the comet in the latitude-independent model is for a parcel of solar

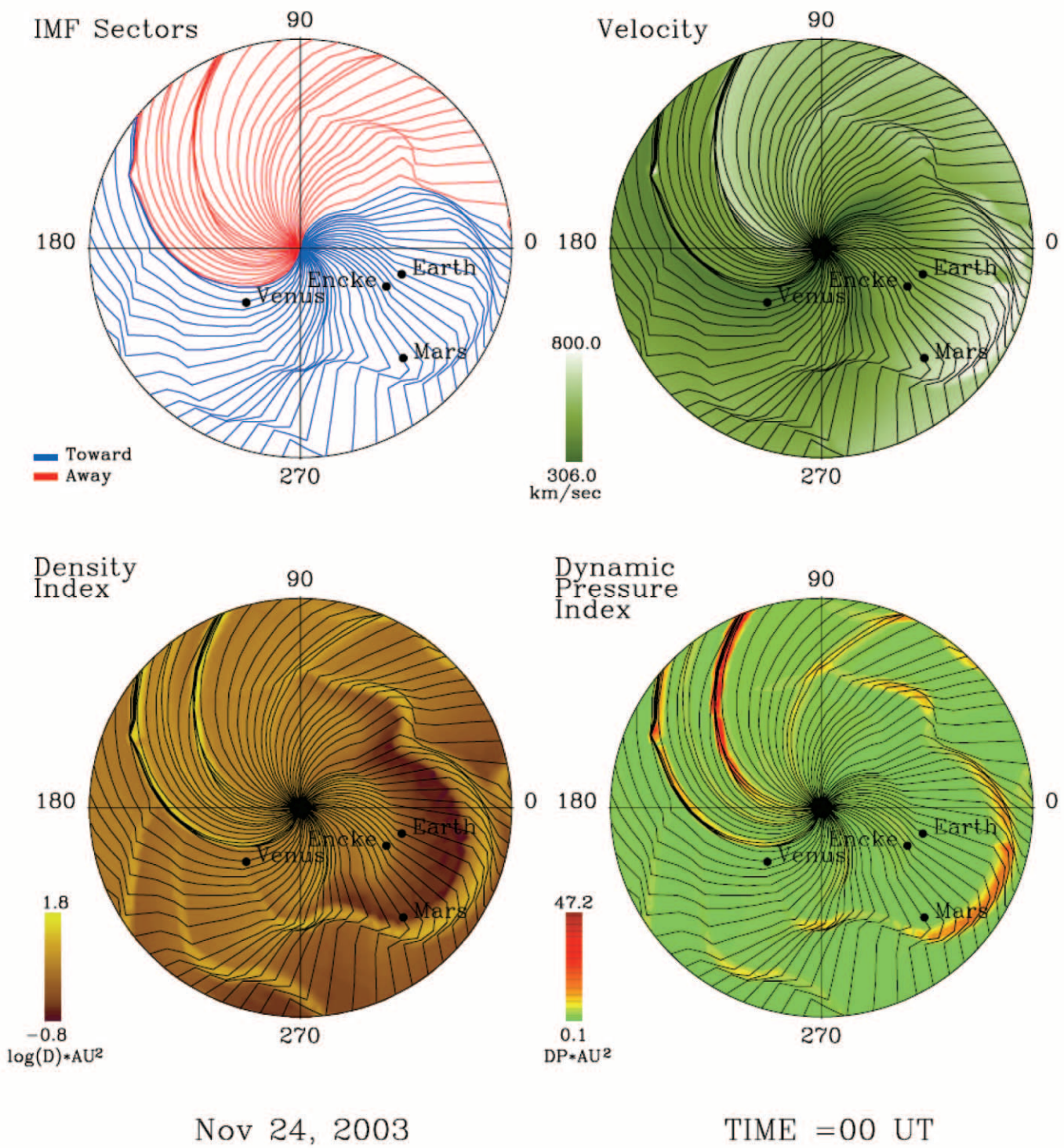

FIG. 4*a*

FIG. 4.—Structure of the interplanetary magnetic field, velocity profiles, and density and dynamic pressure contours. (*a*) Model contours on 2003 November 24 00:00 UT for the ecliptic plane between 0 and 2 AU (Dryer et al. 2004). The view is from the north ecliptic pole. Encke's position 5 hr before the time of the *Chandra* observations, relative to Earth and several planets, is indicated by a small dot. For the duration of the *Chandra* observations, the comet resides in an atypical region of unusual but stable solar wind and magnetic field between two shocks propagating rapidly outward from the Sun. A third shock is beginning to form very close to the Sun. The normal pattern due to Carrington rotation can be seen in the upper left of each figure. (*b*) Same as in (*a*), except 12 hr later at 2003 November 24 12:00 UT. Comparing the models for the two times, the propagation of the quiet region past Encke can be seen. (*c*) Solar wind parameters during the Encke observations. For the geometry of observation, the solar wind at the comet on November 24 encountered the Earth and *ACE*/*SOHO* on November 25, approximately 26 hr later (Table 3). The panels show *ACE* solar wind proton trends during the observations. The solar wind behavior was slowly changing, following a 3 day trend, with a moderate density slowly increasing from 4 to 5 cm^{-3}, a high velocity slowly decreasing from 620 to 550 km s^{-1}, and a thermal temperature decreasing from $\sim 1.5 \times 10^6$ to 1×10^6 K. Assuming that the longitudinal + radial delay model given in the text is correct, the *Chandra* observations should correspond to *ACE* measurements from 02:40 to 17:40 UT on 2003 November 25 (Table 4).

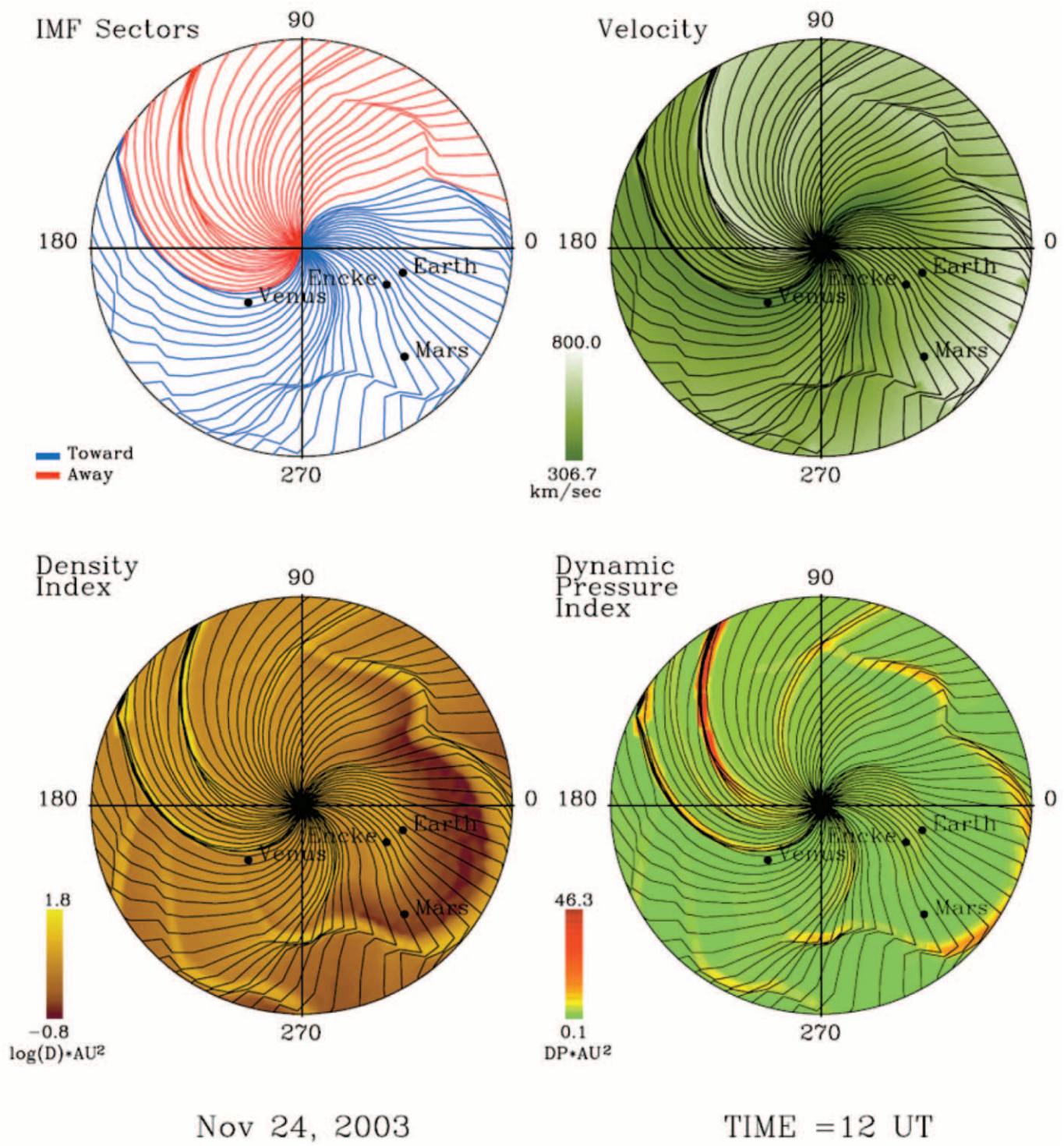

FIG. 4*b*

wind to impact Encke 0.95 days (22.8 hr) before arriving at the Earth (Table 3).

Using this timing, we find from the *ACE* trend data that the solar wind density on 2003 November 24 at the comet was a low 3.5 ± 1.5 cm^{-3}, the solar wind speed was an elevated 600 ± 40 km s^{-1}, and the thermal temperature an abnormally high $(2 \pm 1) \times 10^6$ K, more typical of the high solar corona than normal (Fig. 4*c*). *ACE* charge state ratios for the solar wind are intermediate between the values expected for the slow and fast solar winds (Table 4). This is consistent with a solar wind containing a mix of hot and cold wind material, due to the coronal hole, from the base and top of the corona. The absence of impulsive events in the comet's X-ray light curve is consistent with high-speed solar wind flows. The solar wind parameters as determined by *ACE* are also in good qualitative agreement with the solar wind state as deduced from the Encke X-ray spectrum. The high particle speed directly affects the 380 eV C/560 eV O line ratio in the *Chandra* spectrum, as does the unusual charge

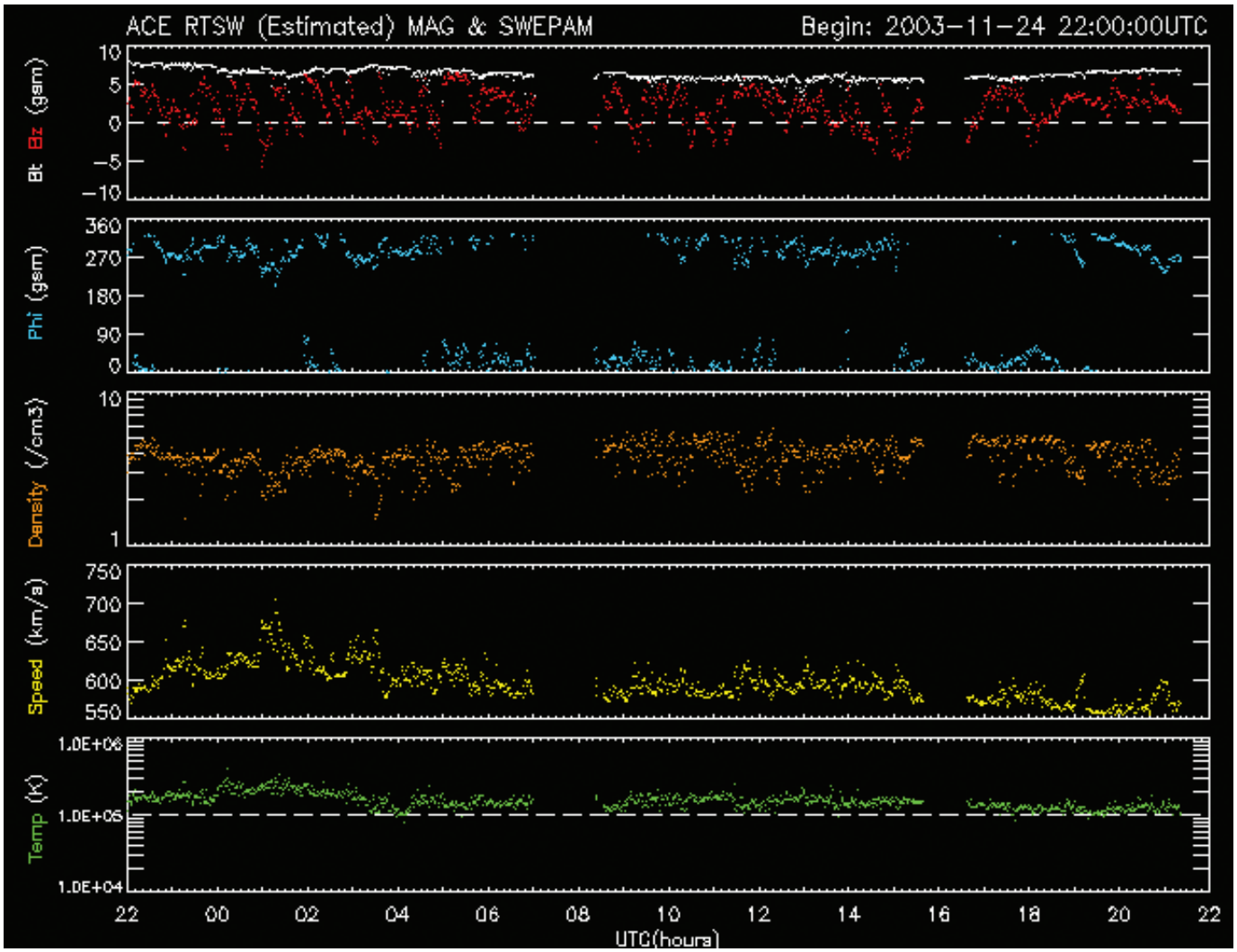

FIG. 4*c*

state, elevating the importance of the carbon lines (Fig. 3). The initial population of excited states (*nl*) following charge exchange is strongly dependent on the collision velocity.

The dominant trend in the solar wind parameters was a gentle cooling and de-acceleration, as the solar wind relaxed from the coronal mass ejection back to the normal parameters for the equatorial wind. We were fortunate that the solar weather was benign and calm during the time of our observations; any major changes over time observed in the X-ray emission were due to something other than variations in the solar wind on a large scale. On the other hand, the weather was "hot" enough so that the Encke X-ray spectrum was unique compared to all other spectra measured to date!

4. DISCUSSION

Morphology.—Compared to our previous observation of comet Encke in 1997 using *ROSAT*, we have succeeded in mapping the X-ray emission around the comet on scales of 500 km in the core,

TABLE 3

SOLAR WIND ARRIVAL TIME DIFFERENCE, COMET AND EARTH

Comet	Observation Time (UT)	$\Delta t_{\rm long}$ (days)	$\Delta t_{\rm radial}$ (days)	$\Delta t_{\rm total}$ (days)	$\Delta t_{\rm observed}$ (days)
Hyakutake	1996 Mar 27	−0.23	0.032	−0.20	0.24
Hale-Bopp	1996 Sep 11	−4.60	5.9	1.30	+1.4
Tempel-Tuttle	1998 Jan 29	−2.31	0.37	−1.94	−2.5
LINEAR S4	2000 Jul 15	+1.2	−0.30 to -0.50	+0.9 to +0.7	−0.25
Encke	1997 Jul 7	−0.26	0.093	−0.17	−0.1
Encke	2003 Nov 24	−0.65	−0.30	−0.95	N/A

NOTES.—Predicted and observed light curve phase shifts using the simple latitude-independent model. The estimated time shifts assume solar wind velocity as measured near Earth. Positive time shifts imply that the solar wind impulse happens at Earth first, comet next. Negative time shifts imply the solar wind boundary hits comet first, Earth next.

TABLE 4
ACE Solar Wind Charge State Ratios during the Encke Observations

Species	*ACE*	Schwadron & Cravens Fast Wind	Schwadron & Cravens Slow Wind
O^{7+}/O^{6+}.....	0.1	0.03	0.27
C^{5+}/C^{6+}.....	2.38	5.18	0.66

Notes.—Measured *ACE* solar wind minor ion charge state ratios on 2003 November 25, as compared to the average ratios for the fast and slow solar winds listed in Schwadron & Cravens (2000). Despite the fact that Encke is a low-latitude comet, where the slow solar wind is expected to dominate, the measured ratios are closer to the average of the fast and slow wind values.

high-signal region near the nucleus and on scales of 1500 km per resolution element throughout the coma. Imaging at these fine scales is unprecedented and is of great interest. Before these observations, it was not known whether the X-ray emission peaks at the position of the nucleus, or "in front" of the nucleus, toward the Sun, within an uncertainty of ~1500 km.

How the X-ray emission relates to the structures within the cometary atmosphere, such as the low Mach number bow shock and the region of plasma exclusion within the cometopause, is also poorly known, although recent work by Wegmann & Dennerl (2005) in detecting the emission morphology discontinuity due to the bow shock region has begun to change this. Assuming an average charge exchange cross section for the coma neutral species of $\sim 3 \times 10^{-15}$ cm^2 and hemispherical outflow for Encke, we find $\tau_{\rm charge\ exchange} \sim 1$ for charge exchange at 1000 km from the nucleus. The minimum *Chandra* resolution element has a width of $\sim 2''$, or 430 km. Thus the observed emission from the comet was collisionally thin to charge exchange except in the central two resolution elements containing the nucleus; this region accounted for less than 0.5% of the total observed emission from the comet. The position of the subsolar bow shock and contact surface for Encke during our observations can be inferred from the P/Halley in situ magnetic field measurements (Neugebauer et al. 1987), scaling the distances by the factor $Q_{\rm gas}$ for each comet, where $Q_{\rm gas}$ is the total production rate of gas from the nucleus (Flammer 1991; Lisse et al. 1999). Using a gas production rate for Halley of 1×10^{30} mol s^{-1} and a bow shock distance of 5×10^5 km (Mukai et al. 1987; Reme et al. 1987), we find for Encke on 2003 November 24 a bow shock distance of 1000 km and the cometopause boundary to be at ~120 km from the nucleus. While these locations are highly contracted compared to other comets due to the low rate of volatile emission and the corresponding low coma density, they should be readily discernible within the *Chandra* images with 430 km spatial resolution. We thus expected to be able to detect them positively in Encke's coma. However, we have not been able to find structures other than a strongly peaked maximum of the emission centered at the nucleus and a fan-shaped structure pointed toward the Sun, both of which mimic the gas coma structure more than anything else.

Or is this simple bow shock–cometopause model of the cometary plasma structure incorrect? In Figure 5 we show the results of a classical magnetohydrodynamic calculation (Gombosi et al. 1996; Häberli et al. 1997) of the interaction of the solar wind with a very asymmetric outgassing comet 2P/Encke. The model calculation assumes a gas production of 8×10^{27} s^{-1}, with 90% of the gas emitted into the sunward side, varying as the cosine of the subsolar angle, and 10% emitted spherically. The ionization rate is 1.3×10^{-6} s^{-1} at a heliocentric distance of 1 AU. The solar wind conditions assumed are a Parker spiral magnetic field with components (−6, 6, 0) nT, a proton density of 4 cm^{-3}, a velocity of 570 km s^{-1}, and a temperature of 1.3×10^6 K. The model-predicted bow shock distance is 25,000 km sunward of the comet and ~50,000 km in the flanks, somewhat larger than we derived from linearly scaling from Halley's $Q_{\rm gas}$ and bow shock position. The cometopause intersects the comet-Sun line at about 120 km sunward of the nucleus and is highly asymmetric. The dark blue interior region corresponds to the diamagnetic cavity, which excludes the outer magnetized solar wind and extends into the long thin ion tail. Comparing to the *Chandra* observations, we do not see an obvious correlation between the modeled plasma structures and the observed X-ray morphology, other than the circular emission region centered on the nucleus and extending out to the minima at 17,000 km ($38''$) radius (Fig. 1), close to the predicted position of the Encke bow shock. There is significant emission outside this radius, and there is no obvious tailward structure. Because the X-ray emission is produced by an interaction between the slowed high charge state solar wind ions and the neutral gas, it is expected that any spatial features associated with the plasma interaction would require an angular resolution smaller than the cometopause distance. Seeing plasma interaction effects for a weak comet such as Encke in an X-ray image may be further complicated by finite (large) gyroradius effects near the bow shock and finite (large) mean free path effects near the cometopause. Both effects tend to smear any strong discontinuities predicted by the pure MHD picture.

If instead we focus on the individual highly charged solar wind ions and their interaction with the neutral gas atmosphere of the comet, we find a very different answer. A detailed, three-dimensional model of the nucleus+coma structure allowing for variable ionization rate of the outflowing coma gas with planar solar wind flow (Bodewits et al. 2004) projected onto the plane of the sky, and compared to the morphological structure found in the $1\farcs5$ resolution Encke X-ray images, is given in Figure 6*a*. In this model, the density distribution of water and its dissociation products is calculated using a standard Haser model with symmetrical hemispherical outflow and outstreaming gas velocity $v = 0.85 r_h^{-1/2}$, where r_h is the heliocentric distance. Evolution of the charge state distribution of the ions is followed as they capture electrons from cometary neutrals. In this model solar wind ions are allowed to penetrate right up to the nucleus; however, given the small size of the cometopause compared with the image resolution, this is not a serious problem. It is assumed that the ions follow straight-line trajectories and have an initial charge state distribution and composition taken from *ACE*. Using velocity-dependent *total* single electron capture cross sections from Fritsch & Lin (1984) and Shipsey et al. (1983), charge state distributions for C^{5+} and C^{6+}, N^{5+} to N^{7+}, and O^{6+} to O^{8+} were calculated. As an example, the charge state distribution for oxygen and carbon ions along the comet-Sun axis is given in Figure 6*b*. It is immediately clear that Encke is collisionally thin to charge exchange, as there is still a significant amount of highly charged oxygen and carbon close to the nucleus.

The chief inputs to this model are the rate of emission of the neutral coma gas, $Q_{\rm gas}$, and the charge state and velocity of the instreaming solar wind. For values of $Q_{\rm gas} \geq 10^{29}$ mol s^{-1}, we recover the "typical" crescent-shaped morphology with maximum offset toward the nucleus. In the collisionally thin regime, for low values of $Q_{\rm gas}$ ($< 10^{28}$ mol s^{-1}) and nominal solar wind properties, the limiting factor is not the number of incoming solar wind minor ions, but the scarce neutral gas coma target molecules. The emission morphology does not show the characteristic crescent shape of the more active comets. Instead, the

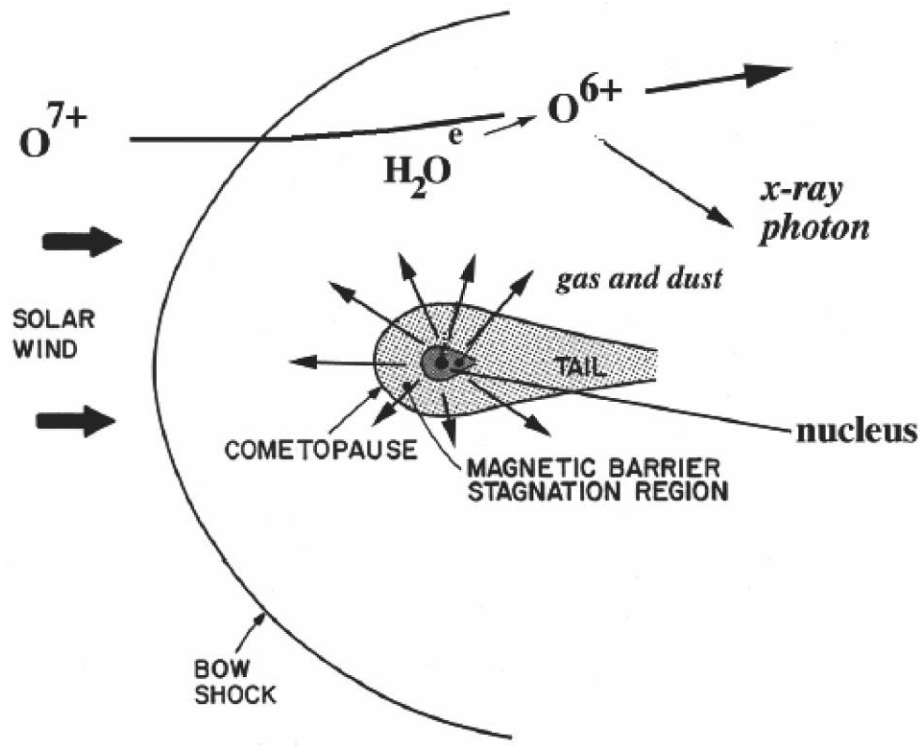

FIG. 5*a*

FIG. 5.—Predicted morphology of the plasma environment around comet 2P/Encke. (*a*) Schematic of the charge exchange interaction, following Cravens (2002). (*b*) Wide view of the plasma density distribution, with the position of the bow shock intersecting the comet-Sun line at about 25,000 km sunward of the nucleus, as predicted from an MHD calculation (Gombosi et al. 1996; Häberli et al. 1997). The values are plotted in the plane containing both components of the Parker spiral interplanetary magnetic field. The draping field lines are also shown. (*c*) MHD predictions of the magnetic field magnitude (*color scale*) and magnetic field line draping (*lines with arrows*) in the vicinity of the cometopause (shown as the yellow-white horseshoe-shaped line that separates the pure cometary ion flow inside from the mass-loaded solar wind flow outside).

model emissivity is a diffuse cloud with a maximum around the nucleus, where the density peaks and traces out the locations of the thin coma gas. Allowing for Encke's very nonsymmetric outgassing morphology, the prediction of a collisionally thin coma with charge exchange occurring wherever there are substantial quantities of neutral coma gas is consistent with the agreement we see between the 2003 images of the observed X-ray morphology and the optical coma (Fig. 1).

Comparing our 2003 *Chandra* observations to the 1997 *EUVE*/*ROSAT* observations of the comet, we find very different morphologies for the X-ray emission. The 1997 observations demonstrated the "classical" crescent-shaped emission pattern in the sunward half of the coma, produced by a collisionally thick interaction between the solar wind and the coma. Both times the comet was observed within 0.3 AU of the Earth, and the estimated *SOHO* water production rates were the same within a factor of 2.5 (T. Mäkinen 2004, private communication). The major difference seems to be that the 2003 observations were taken pre-perihelion, with cometary activity mainly found in the directed emission produced by two jets plus a weak fan (Figs. 1*b* and 1*c*), while in 1997 the observations were taken after the comet had been thoroughly heated by a perihelion solar passage and a relatively dense, spherical coma had formed (Fig. 1*d*). Even allowing for the different observational capabilities of the *ROSAT* and *Chandra* X-ray cameras, these differences are real. Evidently, an important change in the observed morphology occurs at $Q_{\rm gas} \sim 10^{28}$ mol s^{-1}. We do find it surprising, however, that such large changes in behavior happen for only a factor of 2.5 difference in $Q_{\rm gas}$.

Total X-ray luminosity.—As a check, we adopt the simple charge exchange model of Cravens (1997) to determine whether charge exchange is a plausible mechanism for the observed emission. From the model, we have $L_{\rm X} \sim 4.0 \times 10^{-21} N_{\rm neutral} N_{\rm SW} \times (v_{\rm SW}/400 \text{ km s}^{-1}) V$ ergs s^{-1}. For Encke, using a hemispherical volume V of radius 40,000 km, a spherical gas outflow at $v_{\rm gas} = 0.8$ km s^{-1} and $Q_{\rm gas} = 7.3 \times 10^{27}$ s^{-1} (Table 1), and a *SOHO* solar wind density outside the bow shock of $\sim$4 cm^{-3}, we find a total X-ray luminosity for the comet of $\sim 2.8 \times 10^{14}$ ergs s^{-1}. This value is consistent with the measured 3.8×10^{14} *Chandra* luminosity, within the errors of the Cravens model ($\pm$100%).

Temporal variations.—None of the impulsive events found in our previous observations of comets was seen (Lisse et al. 1996, 1999, 2001; Table 3). The solar wind flow in high-speed streams is known to be rather smooth, whereas the slow flow more typical near the ecliptic plane is known to be more turbulent (McComas et al. 1998). The 15 hr duration of the observations may have been too short to expect a solar wind sector boundary crossing (period $\sim$ 7 days) while we were conducting the *Chandra* observations. The 1997 *ROSAT*/*EUVE* observations demonstrated a 25% duty cycle for the impulses over a 2 week time span.

In terms of our experimental goal of finding X-ray periodicity due to modulation of the coma by a rotating, asymmetric nucleus, we were extraordinarily lucky in our time of observation and choice of target: the solar wind was relatively stable over the time of our observations (Fig. 4*c*). K. Dennerl (1998, private communication) reported statistically significant variations in the X-ray emission morphology from comet C/Tabur 1996 Q1, as observed by *ROSAT*, on length scales of $\sim 10^3$–10^4 km.

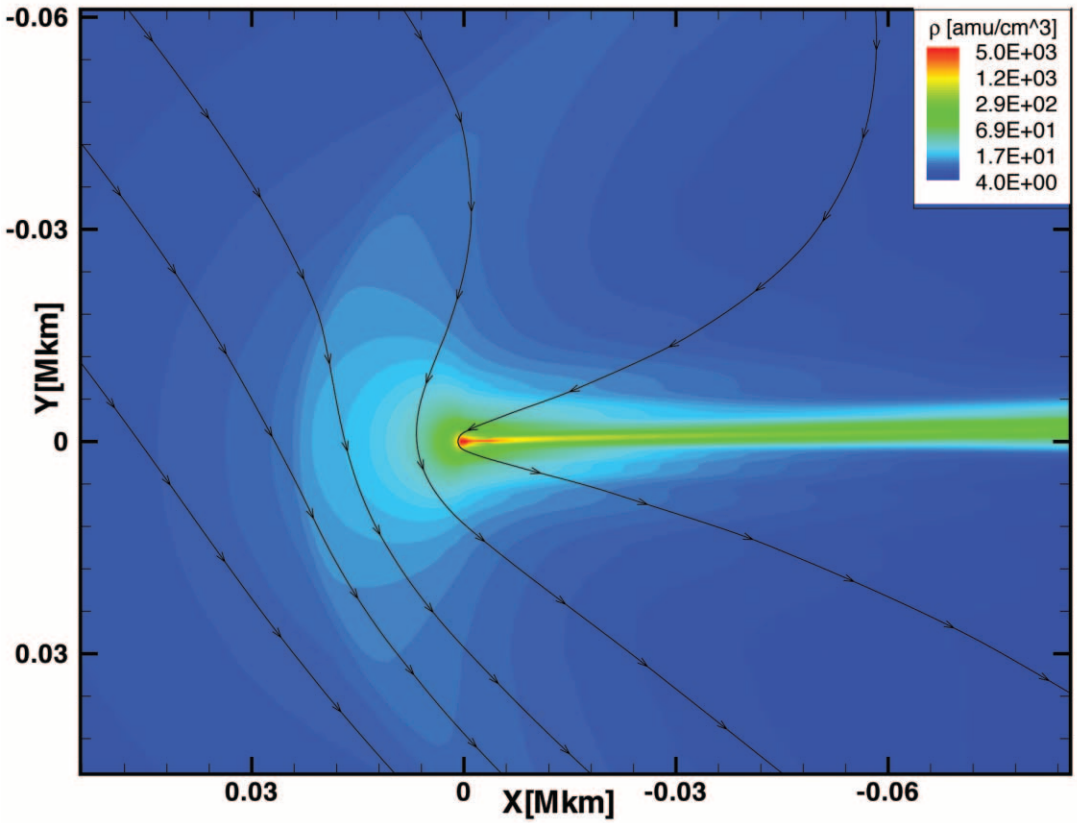
ρ [amu/cm^3]
5.0E+03
1.2E+03
2.9E+02
6.9E+01
1.7E+01
4.0E+00
-0.06
-0.03
0
0.03
Y[Mkm]
0.03
0
X[Mkm]
-0.03
-0.06

FIG. 5*b*

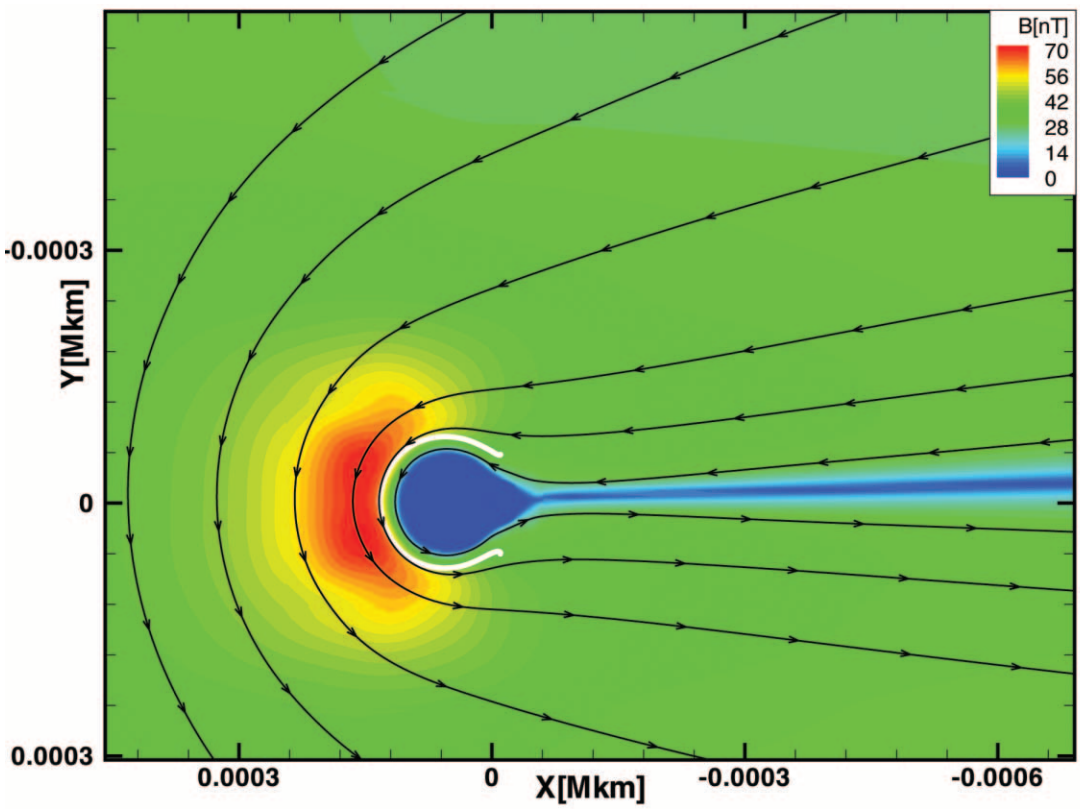
B[nT]
70
56
42
28
14
0
-0.0003
0
0.0003
Y[Mkm]
0.0003
0
X[Mkm]
-0.0003
-0.0006

FIG. 5*c*

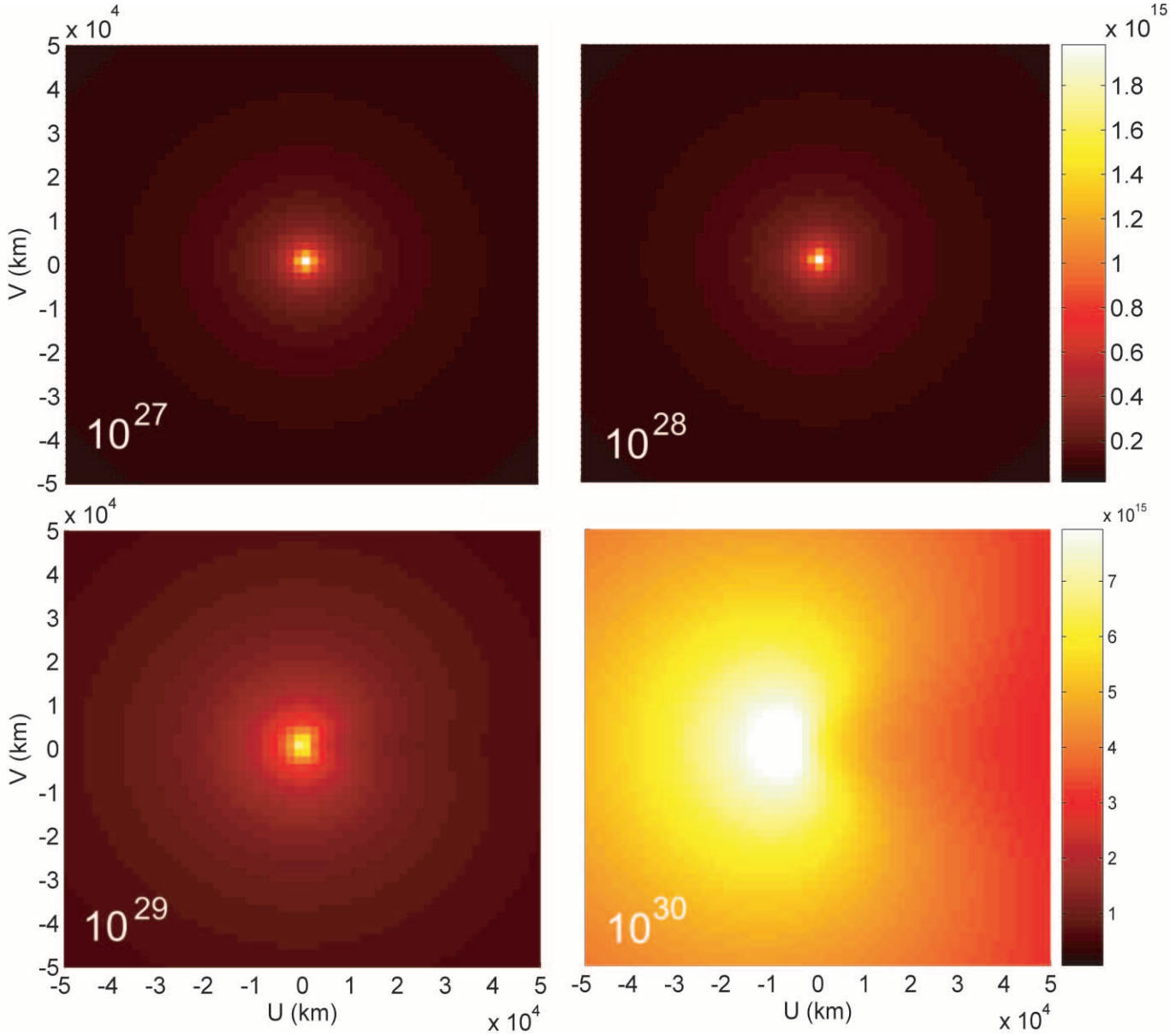

FIG. 6*a*

FIG. 6.—Predicted morphology for the X-ray emission from comet Encke. (*a*) Morphology as a function of comet gas production rate, following Bodewits et al. (2004). Note the decreasing concentration of model source function and the increasing importance of diffuse halo emission in the extended coma as the gas production rate increases. (*b*) Model neutral gas density distributions for the dominant neutral species, water and its dissociation products, in the coma of Encke. (*c*) Predicted oxygen and carbon charge state distribution in the coma of Encke along the comet-Sun axis from the Bodewits model, using the *ACE* initial charge state distribution given in Table 4.

Images of Tabur's coma taken hours apart show knots of emission lighting up in different locations at different times. Small regions of apparent enhanced brightness a few arcseconds in extent were also found using *Chandra* for C/1999 S4 (LINEAR) and C/McNaught-Hartley (2001), but were not statistically significant above the 2 σ level. Because of the compact nature of the emission region, the time for crossing of the coma by gas emitted from the nucleus is on the order of 12 hr, and by the solar wind is on the order of a few minutes.

We find good agreement between our observed X-ray light curve and the newly refined 11.1 hr nucleus rotation period of Fernández et al. (2005; our Fig. 2*a*). Belton et al. (2005) also find an 11.2 hr best-fit period for the rotation of the comet. In their earlier work, Luu & Jewitt (1990) also found an 11 or 22 hr periodicity possible but argued for a 15 hr phasing as more likely. From the X-ray data, we can rule out periods shortward of 9 hr and longward of 12 hr. Returning to the low-level or "baseline" emission time series for the 1997 *EUVE*/*ROSAT* light curve of Encke, we find peaks in the power spectrum at ~23 hr. The power spectrum is noisy, though, and we cannot determine whether an 11 hr period would fit the data, due to the sparseness of the light curve sampling. We can, however, state that the 11.1 hr period here is consistent with the 1997 pre-outburst measurements.

It is possible that our light curve is influenced by fluctuations in the solar wind or incorrectly removed variations in the background signal of the detector. However, examining the background signal in the ACIS-S data, and the *SOHO* Proton Monitor solar

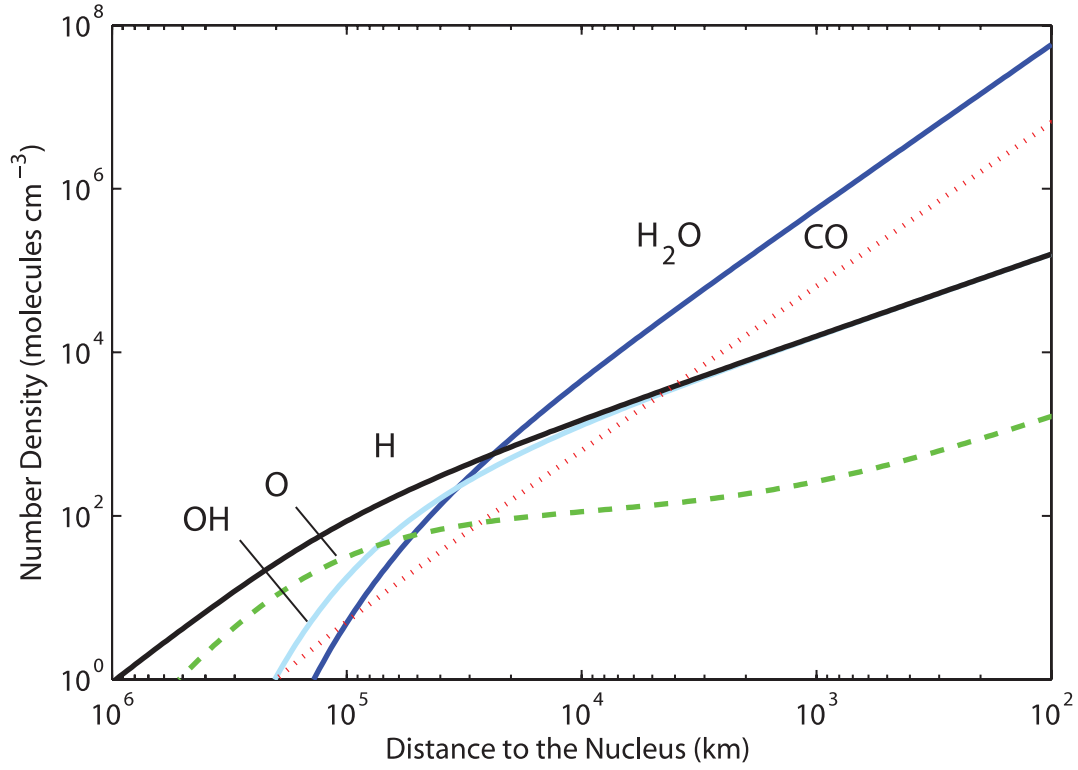
Number Density (molecules cm^{-3})
Distance to the Nucleus (km)
H_2O
CO
H
O
OH

FIG. 6*b*

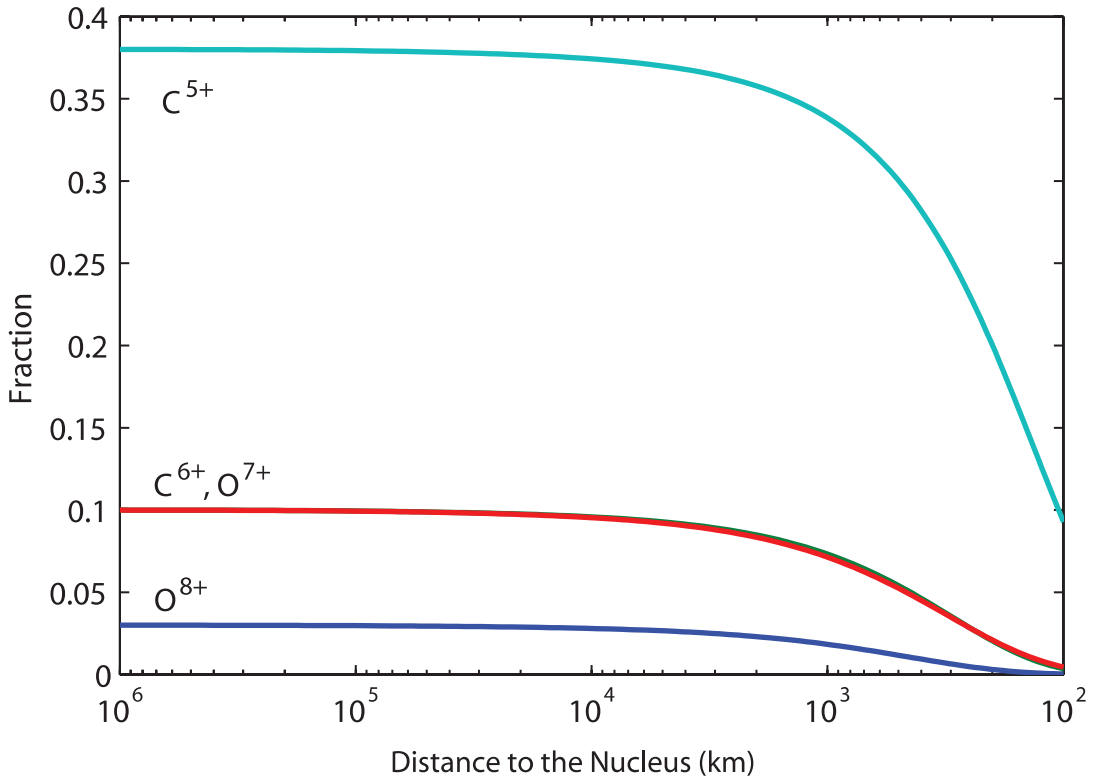
Fraction
Distance to the Nucleus (km)
C^{5+}
C^{6+}, O^{7+}
O^{8+}

FIG. 6*c*

wind proton flux trends over the time share of our observations, we find no trends in the background and only a linear secular decrease in the solar wind flux. The dust and gas emission behavior with time and heliocentric distance have been well documented by Sekanina (1988a, 1988b) and Mäkinen et al. (2001) and shown to have asymmetric, seasonal behavior caused by localized, rotationally variable regions of emission on the surface. Physically, we estimate that for $\sim$1 km s^{-1} gas emission speeds *and* a core X-ray emission region with greater than 50% of the total emission in a region less than 18,000 km in radius, asymmetric emission patterns of gas from the surface of the nucleus can modulate the structure of the comet's atmosphere, and hence its X-ray emission pattern, on timescales of less than one-fifth of a day.

Charge state ratios.—We expect softer photons near the nucleus, as the solar wind traverses the coma and its net ionization is reduced; this effect was measured in situ by the *Giotto* probe during its 1986 flyby of comet 1P/Halley (Fuselier et al. 1991). The most prominent X-ray lines are due to oxygen, so we have studied the O VII/O VIII ratio. (While O^{6+} is the most abundant oxygen ion in the solar wind, only O^{+8} and O^{+7} concern us here, as only O VIII and O VII emission, created when O^{+8} and O^{+7} charge exchange, fall in the X-ray region of the spectrum.) From our spatial model of the charge state distributions for Encke (Fig. 6*c*), because of the collisionally thin nature of the system, we do not expect any appreciable variation in the O^{+7}/O^{+8} ratio, and hence in the observed O VII/O VIII line emission, at distances >1000 km from the nucleus. Unfortunately, the effective spatial resolution and count rate of the Encke imagery are too low to allow us to determine the spatial dependence of the O^{+7}/O^{+8} ratio. A search for variations in the O VII/O VIII line ratio due to reduction of the solar wind as it traverses the gas coma was also inconclusive for C/1999 S4 (LINEAR), but a clear trend of increasing O VII/O VIII emission toward the nucleus was found in our reanalysis of the *Chandra* observations of C/McNaught-Hartley 2001 (Krasnopolsky et al. 2002). It is not clear whether the difference in the two results is due to overfilling of the S3 chip by C/1999 S4 (LINEAR) in 2000 July or due to variability in the solar wind O^{+7}/O^{+8} abundance. Neugebauer et al. (2000) argue that the O^{+7}/O^{+8} ratio is highly variable in the solar wind, so that the changing ratio of O^{+7}/O^{+8} in the coma of C/McNaught-Hartley 2001 and the relatively constant ratio found in C/1999 S4 (LINEAR) may simply be due to a much smaller initial amount of O^{+7} in the solar wind impacting the coma of C/McNaught-Hartley 2001. From the *Chandra* X-ray spectra, the comets appear to be encountering very different O^{+7}/O^{+8} solar wind compositions, as evidenced from the 560 eV/660 eV line ratios (Fig. 3*c*).

Charge exchange spectral model.—Several spectral models are now available to simulate the observed X-ray emission. Here we employ the model of Bodewits et al. (2004) to include the properties of both the neutral comet (spatial density, composition) and the ionized solar wind (speed, composition, spatial density) in determining the behavior of the X-ray emission. In this first results paper, the model is used to broadly understand the plethora of new phenomena seen in the 2003 November *Chandra* observations of Encke and to show that they arise from a common source. In a follow-up paper, a highly detailed spectral analysis will be presented.

As described above, our model promulgates a detailed morphological model of the neutral coma interacting with the planar flow of the incoming solar wind, yielding a two-dimensional X-ray emissivity. A three-dimensional integration assuming cylindrical symmetry around the comet-Sun axis viewed from the observer's phase angle in turn yields the absolute intensity of cometary emission lines (Fig. 6*a*). Effects of the *Chandra* instrument response were simply modeled by assuming a spectrometer resolution of 60 eV and the Cycle 5 effective areas (*Chandra* Observer's Manual, Ver. 4.0). To arrive at a spatially dependent spectrum, cascade spectra have to be calculated for all the ions included in the model. Care has been exercised in using velocity-dependent, *state-selective* electron capture cross sections for atomic hydrogen from Fritsch & Lin (1984) and Shipsey et al. (1983). Forbidden lines are included, assuming a triplet/singlet ratio of

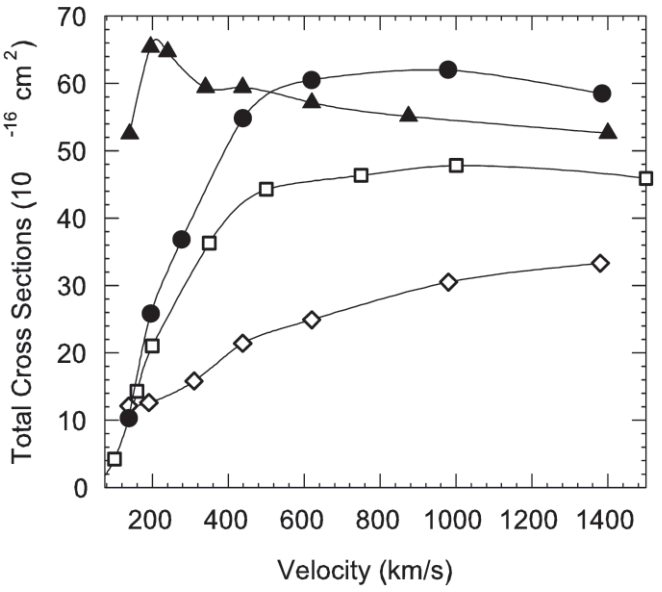

FIG. 7*a*

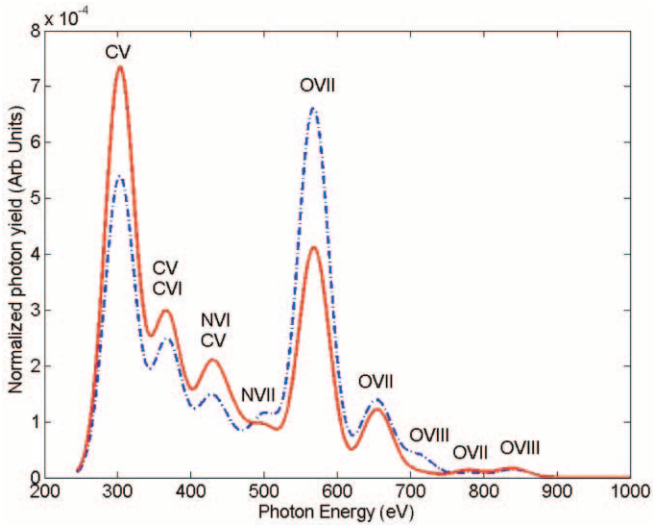

FIG. 7*b*

FIG. 7.—(*a*) Total cross sections for charge exchange of an electron between a highly charged ion and a cometary neutral, as a function of relative ion velocity. Cross sections are given in units of 10^{-16} cm^{-2}, the hard sphere cross section for a hydrogen atom. Filled triangles denote the cross sections for O^{+8}, filled circles the cross sections for O^{+7}, diamonds the cross sections for C^{+5}, and squares the cross sections for C^{+6}. The largest relative change over the range of observed solar wind ion speeds occurs for the C^{+6} and O^{+8} ions. (*b*) Encke X-ray spectra for two different solar wind speeds, assuming a resolution of 60 eV, for the collisionally thin case. *Blue curve*: The 200 km s^{-1} solar wind speed. *Red curve*: The 600 km s^{-1} solar wind speed. The largest changes in the spectra occur near 350, 500, 650, and 820 eV.

3:1. Multiple electron capture, which tends to increase Lyα lines, is not included in the model. To get absolute intensities, a solar wind heavy-ion flux of 1.70×10^5 ions cm^{-2} s^{-1} was assumed.

The as-observed line intensities from the best-fit XSPEC eight emission line fit to the data are presented in Figures 3*a* and 3*b*. Using solar wind velocities of 600 km s^{-1} (the measured velocity during the Encke observations from *ACE* data) and 200 km s^{-1} (typical of the slow, thick solar wind at low heliographic latitudes/in the ecliptic), velocity-dependent charge exchange cross sections (Fig. 7*a*), and charge state ratios for the fast and slow solar winds from Schwadron & Cravens (2000), from first principles we have simulated the emission spectra (Fig. 7*b*). It is immediately clear that the Encke spectra are most similar to the 600 km s^{-1} model, consistent with the *ACE* and *SOHO* solar wind speed and temperature measurements. The dominant cause of the highly elevated C/O line ratios is due to the highly elevated cross section for C^{+6} charge exchange at 600 km s^{-1}. The high particle speed directly affects the 380 eV C/560 eV O VII line ratio in the *Chandra* spectrum, as does the unusual charge state, elevating the importance of the carbon lines (Fig. 3*c*). The initial population of excited states (*nl*) following charge exchange is strongly dependent on the collision velocity. The solar wind densities as determined by *ACE* are also in good qualitative agreement with the solar wind state as deduced from the Encke X-ray spectrum.

New lines.—Because the Encke–solar wind system was collisionally thin to charge exchange at $Q_{\rm gas} < 10^{28}$ mol s^{-1}, the spectrum may allow for new line detections. That is, for oxygen the collisionally thin spectrum is not "filled in" by all possible emission in the O VII and O VIII lines, while the less abundant species with higher cross sections for charge exchange are still near their maximum possible luminosity (Fig. 6*c*). Emission due to Ne and Fe, which are both abundant in the solar wind, should be found at 826 eV (Fe XVII), 880 eV (Fe XVIII), and 940 eV (Ne IX). While there is an apparent peak at 826 eV in our *Chandra* spectrum (Fig. 3), we cannot claim a definitive detection of an Fe line, as there is a stronger O^{+8} line at 796 eV and there is no obvious need for two lines in the XSPEC modeling of the data at greater than 3 σ statistical significance. We do find a 5 σ line at an energy of 984 eV, which we assign to Ne IX. Ne IX emission barely fell below the background sensitivity limit for C/1999 S4 (LINEAR) (Lisse et al. 2001) and was detected in C/McNaught-Hartley 2001 by Krasnopolsky et al. (2002) with line center at ~960 eV.

Emission due to charge exchange by another abundant solar wind species, N^{+6}, should be present but is very hard to resolve. The Bodewits spectral model demonstrates why it is so hard to detect N VI versus C VI: on a per atom basis, the nearby C VI lines are much stronger than the nitrogen lines. C VI emission alone would produce a 380 eV/450 eV line ratio of 4.0, as opposed to the observed ratio of 3.0 $\pm$ 0.6 (2 σ). While highly interesting, we can at most claim this as a tentative detection of N VI emission, worthy of further study but not yet conclusive. A similar conclusion was found by P. Beiersdorfer (2003, private communication) in fitting the *Chandra* C/1999 S4 (LINEAR) X-ray spectra to laboratory electron-ion trap measurements of charge exchange emission by helium-like and hydrogen-like C, N, and O.

5. CONCLUSIONS

Comet Encke was observed on 2003 November 24 for 15 continuous hours using the *Chandra* ACIS-S imaging spectrometer. Compared to observations of other comets, the *Chandra* results were unusual:

1. The coma of the comet was clearly collisionally thin to charge exchange with the solar wind up to the central pixel containing the nucleus. The "typical" crescent-shaped emission region was not found. Instead, X-ray emission from comet Encke was resolved on scales of 500–40,000 km, with unusual morphology due to the presence of a low-density, collisionally thin (to charge exchange) coma.
2. A light curve with a peak-to-peak amplitude of 20% and a period 10.5 $\pm$ 1.5 (2 σ) hr was found over the 15 hr observing period, consistent with recent evaluations of the nuclear rotation period of ~11 hr (Fernández et al. 2005; Belton et al. 2005). Without a collisionally thin coma, modulation of the X-ray signal by variable nuclear gas emission would not affect the charge exchange interaction, except over the largest scales where the effects are moderated and diluted.
3. A spectrum dominated by charge exchange emission from solar wind C, O, Ne, and possibly N ions was obtained. The measured and inferred charge state of the solar wind for this low-latitude comet was unusually "cold." Very unusual oxygen and carbon line ratios were seen in the 200–700 eV range. There was a marked absence of impulsive variations of the X-ray emission and changes in the solar wind flux during the observations, and the solar wind speed was very high, ~600 km s^{-1}.

These findings are consistent with the moderate emission rate of neutral gas from Encke (~7×10^{27} mol s^{-1}) and contemporaneous measurements of the solar wind made by *SOHO* and *ACE* showing dominance of the inner heliosphere by a postshock bubble of expanding solar wind plasma containing material from throughout the corona, mixing the behavior seen in high and low heliographic latitude solar wind flow.

The *SOHO* CELIAS heavy-ion and MTOF Proton Monitor data were graciously provided by the University of Maryland *SOHO* project, http://umtof.umd.edu/pm. The *SOHO* SEM solar X-ray monitor data are used courtesy of H. Ogawa at the University of Southern California, http://www.usc.edu/dept/space_science/semdata.htm. The Encke gas production rates were derived by T. Mäkinen from *SOHO* SWAN observations, and the Encke gas and dust coma images were supplied courtesy of D. Schleicher and L. Woodney. The *ACE* solar wind heavy-ion data were obtained courtesy of T. Zurbuchen and J. Raines of the University of Michigan and of the *ACE* SWICS team, http://www.srl.caltech.edu/ACE. We are grateful for the cometary ephemerides of D. K. Yeomans et al. found at http://ssd.jpl.nasa.gov/horizons.html used to reduce our data. Help with the MHD modeling was provided by Y. Jia at the University of Michigan. C. Lisse was supported in part by SMAO observing grants NAG GO45167X, and D. Bodewits and R. Hoekstra would like to acknowledge support within the FOM-EURATOM association agreement.

REFERENCES

Arnaud, K. A. 1996, in ASP Conf. Ser. 101, Astronomical Data Analysis Software and Systems V, ed. G. H. Jacoby & J. Barnes (San Francisco: ASP), 17
Beiersdorfer, P., et al. 2003, Science, 300, 1558
Belton, M., et al. 2005, Icarus, 175, 181
Bodewits, D., Juhasz, Z., Tielens, A. G. G. M., & Hoekstra, R. 2004, ApJ, 606, L81
Cravens, T. E. 1997, Geophys Res. Lett., 24, 105
———. 2002, Science, 296, 1042
Dennerl, K., et al. 1997, Science, 277, 1625
Dryer, M. 1998, AIAA J., 36, 365
Dryer, M., et al. 2001, Sol. Phys., 204, 265
———. 2004, Space Weather, 2, 9001

Fernández, Y. R., et al. 2005, Icarus, 175, 194
Festou, M., & Barale, O. 2000, AJ, 119, 3119
Flammer, K. 1991, in Comets in the Post-Halley Era, ed. R. L. Newburn, M. Neugebauer, & J. Rahe (Dordrecht: Kluwer), 1125
Fritsch, W., & Lin, C. D. 1984, J. Phys. B, 17, 3271
Fry, C., et al. 2001, J. Geophys. Res., 106, 20985
———. 2003, J. Geophys. Res. 108(A2), 1070
———. 2004, IEEE Trans. Plasma Phys., 32(4), 1489
Fuselier, S., et al. 1991, ApJ, 379, 734
Gombosi, T., et al. 1996, J. Geophys. Res., 101, 15233
Häberli, R., et al. 1997, Icarus, 130, 373
Kharchenko, V., & Dalgarno, A. 2000, J. Geophys. Res., 105, 18351
———. 2001, ApJ, 554, L99
Kharchenko, V., et al. 2003, ApJ, 585, L73
Krasnopolsky, V., et al. 2002, Icarus, 160, 437
Lisse, C. M., & Christian, D. J. 2002, in ASP Conf. Ser. 264, Continuing the Challenge of EUV Astronomy: Current Analysis and Prospects for the Future, ed. S. B. Howell, J. Dupuis, D. Golombek, F. M. Walter, & J. Cullison (San Francisco: ASP), 254
Lisse, C. M., Cravens, T. E., & Dennerl, K. 2004, in Comets II, ed. M. C. Festou, H. A. Weaver, & H. U. Keller (Tucson: Univ. Arizona Press), 631
Lisse, C. M., et al. 1996, Science 274, 205
———. 1999, Icarus, 141, 316
———. 2001, Science, 292, 1343
Luu, J., & Jewitt, D. 1990, Icarus, 86, 69
Mäkinen, T., et al. 2001, Icarus, 152, 268
McComas, D., et al. 1998, Geophys. Res. Lett., 25, 1
Mukai, T., et al. 1987, A&A, 187, 129
Neugebauer, M., et al. 1987, A&A, 187, 21
———. 2000, J. Geophys. Res., 105, 20949
Reme, H., et al. 1987, A&A, 187, 33
Schwadron, N., & Cravens, T. E. 2000, ApJ, 544, 558
Sekanina, Z. 1988a, AJ, 95, 911
———. 1988b, AJ, 96, 1455
Shipsey, E., et al. 1983, Phys. Rev. A, 27, 821
Wegmann, R., & Dennerl, K. 2005, A&A, 430, L33
Wegmann, R., Dennerl, K., & Lisse, C. M. 2004, A&A, 428, 647